*Physics – Uspekhi* **52** (9) 945 – 971 (2009) 

*CONFERENCES AND SYMPOSIA*

PACS numbers: **02.70.–c**, 36.40.Gk, 42.25.Fx, 42.25.Gy, **42.55.–f**, 42.70.Qs, **71.36.+c**, 73.20.Mf, 78.20.Ls, **78.67.–n**

# Nanoplasmonics and metamaterials
# (Scientific session of the Division of Physical Sciences, Russian Academy of Sciences, 27 April 2009)

S G Tikhodeev, N A Gippius; T V Shubina, S V Ivanov, A A Toropov, P S Kop'ev; V V Kurin; A N Lagarkov, A K Sarychev; N A Gippius, S G Tikhodeev

DOI: 10.3367/UFNe.0179.200909g.1003

On 27 April 2009, in the conference hall of the Lebedev Physical Institute, Russian Academy of Sciences, a scientific session of the Division of Physical Sciences of the Russian Academy of Sciences devoted to the problem of nanoplasmonics and metamaterials took place. The following reports were presented at the session:

(1) **Tikhodeev S G, Gippius N A** (Prokhorov Institute of General Physics, Russian Academy of Sciences, Moscow) "Plasmon–polariton effects in nanostructured metal–dielectric photonic crystals and metamaterials";

(2) **Shubina T V, Ivanov S V, Toropov A A, Kop'ev P S** (Ioffe Physicotechnical Institute, Russian Academy of Sciences, St. Petersburg) "Plasmon effects in In(Ga)N-based nanostructures";

(3) **Kurin V V** (Institute of Physics of Microstructures, Russian Academy of Sciences, Nizhnii Novgorod) "Resonance scattering of light in nanostructured metallic and ferromagnetic films";

(4) **Lagarkov A N , Sarychev A K** (Institute of Theoretical and Applied Electrodynamics, Joint Institute of High Temperatures, Russian Academy of Sciences, Moscow) "Active optical metamaterials";

(5) **Gippius N A, Tikhodeev S G** (Prokhorov Institute of General Physics, Russian Academy of Sciences, Moscow) "Application of the scattering matrix method for calculating the optical properties of metamaterials."

Summaries of reports 1–3 and 5 and of an article written on the basis of report 4 are given below.

PACS numbers: 42.70.Qs, **71.36.+c**, 73.20.Mf
DOI: 10.3367/UFNe.0179.200909h.1003

## Plasmon–polariton effects in nanostructured metal–dielectric photonic crystals and metamaterials

S G Tikhodeev, N A Gippius

In this report, we give a brief introduction to nanoplasmonics, the optical properties of plasmon–polariton photonic crystals, and metamaterials. In more detail, we analyze the problem of determining the effective electromagnetic response of thin layers of metamaterials of an arbitrary symmetry, including gyrotropic ones.

Surface plasmons are collective oscillations of conduction electrons of a metal excited by light near its surface — the interface with a dielectric. Depending on the geometry of the metal–dielectric structure, localized plasmons (in metal clusters or pores inside metal with a size much smaller than the wavelength of light, i.e., in nanoclusters) and delocalized surface plasmons (on an infinite flat metal–dielectric interface) are distinguished. However, even in the case of delocalized plasmons, their excitation by light requires that the metal surface be nanostructured. Therefore, this thriving field of physics is frequently called *nanoplasmonics*.

In fact, nanoplasmonics has very long been used by humankind. The localized plasmons in silver and gold nanoclusters in glass ensure the extraordinary brightness and longevity of the colored stained-glass windows of medieval cathedrals. We can remember an even older example — the famous Lycurgus Cup, which was made, apparently, in Rome in the 4th century A.D. (now in the British museum); it is also made from glass with metallic nanoclusters. However, the truly thriving development and application of nanoplasmonics started only recently in connection with the development of nanotechnology and computational electrodynamic methods [1–5].

Nanoplasmonics is attractive, first of all, because plasmons allow concentrating electromagnetic energy in small volumes (in comparison with the wavelength of light). Plasmons, having a giant dipole moment, are efficient mediators in the interaction of these small volumes with light. Furthermore, the properties of plasmons can be controlled in extremely wide limits.

A detailed survey of the achievements of nanoplasmonics is beyond the scope of this report. We only mention here that one of the basic methods of controlling plasmons is constructing so-called polaritonic crystals. Polaritonic crystals are artificial periodic media, in which optically active electronic resonances exist together with photonic resonances (which arise due to a periodic modulation of a dielectric constant). The coupled photonic and electronic resonances are conventionally called polaritons; therefore, photonic crystals with interacting electronic and photonic resonances are now called polaritonic crystals. Initially, photonic crystals made of transparent dielectrics with light-frequency-independent dielectric constants were studied [6–9]. In the first polaritonic crystals, Bragg superlattices of

*Uspekhi Fizicheskikh Nauk* **179** (9) 1003 – 1030 (2009)
DOI: 10.3367/UFNr.0179.200909g.1003
Translated by S N Gorin; edited by A M Semikhatov

semiconductor quantum wells were used [10, 11]. The role of electronic resonances was then played by excitons in the quantum wells. Later, exciton–polariton crystals with another geometry were proposed, in the form of so-called photonic-crystal slabs [12–14], i.e., planar waveguide layers modulated by one-dimensional or two-dimensional lattices, e.g., of depressions filled with a layered semiconductor with strong excitonic resonances.

But polaritonic effects in modulated metal–dielectric structures proved to be most interesting. The role of electronic resonance is there played by localized or surface plasmons. The first samples of such 'polaritonic crystalline layers' were investigated more than a hundred years ago; however, they had a different name then, diffraction gratings. The first plasmon–polariton effects were the resonance anomalies found by Wood [15] in the optical spectra of lattices created on the surface of a metal, and first explained by the excitation of surface plasmons by Fano [16].

Subsequently, significant attention has been given to these structures due to the detection of so-called anomalous light transmission through a lattice of subwavelength holes in a metal layer [17]. We also note the formation of plasmon–waveguide polaritons in lattices of metallic nanoclusters or nanowires on the surface of a planar dielectric waveguide [18, 19], as well as interesting plasmonic effects in metal layers with lattices of voids [20, 21].

It was recently revealed that when using ferromagnetic materials (for preparing either a dielectric waveguide or nanoclusters), extremely interesting magnetooptical effects potentially important in applications [22, 23] appear in such systems.

But the greatest burst of interest in metal–dielectric polaritonic crystals arose in connection with the possibility of designing artificial media, so-called metamaterials with a controlled electromagnetic response, on their basis. Among the possibilities discussed are metamaterials with a negative refractive index [24] for creating unconventional new optic devices and new methods of controlling light [3, 25–31].

A medium with a negative refractive index must have negative dielectric and negative magnetic constants (a more precise formulation for absorbing media: different signs of the real and imaginary parts of the refractive index.) The negative sign of the dielectric constant is ensured by the use of a metal. To ensure a negative magnetic susceptibility, structurization is required; it is necessary to ensure a magnetoinductive resonance, which requires the presence of circular current contours. A medium with a negative refractive index was first realized for the microwave range with the aid of split ring resonators [26]. Then it was understood [27] that in the near-infrared and visible optical ranges, the role of ring contours for the current can be played by coupled localized plasmons, for example, based on double-chain metallic nanowires. Metamaterials have been proposed based on pairs of periodically perforated metallic layers, so-called fishnet structures [28, 32], and media with a strong natural optical activity [31, 33, 34] and with strong optical nonlinearities [35, 36] have been created.

Metamaterials are short-period metal–dielectric plasmonic crystals. The idea consists in the period of the metamaterial being less than the relevant wavelength of light. Then the layer of the metamaterial in the far wave zone behaves as a layer of a uniform substance; there is no diffraction, only transmission, reflection, and absorption of light. The question of correctly describing the effective electromagnetic response of metamaterials is therefore very important [37, 38]. One of the methods to obtain the effective dielectric and magnetic susceptibilities ($\varepsilon$ and $\mu$) of a metamaterial is the parameterization of the experimentally measured or theoretically calculated coefficients of transmission and reflection of a finite-thickness layer of a metamaterial [39, 40]. Below, we briefly describe the scheme of this parameterization, which becomes highly nontrivial in the case of a metamaterial of lowered symmetry.

It is known that for a complete description of the electromagnetic properties of a homogeneous medium (including one without an inversion center, i.e., gyrotropic), it is sufficient to introduce the nonlocal dielectric constant tensor $\varepsilon_{ij}(\omega, \mathbf{k})$ and to assume that $\mu = 1$ [37]. Such a description — with the aid of a nonlocal dielectric susceptibility — includes, as a special case, the traditional approach to nongyrotropic media with the use of local $\varepsilon_{ij}(\omega)$ and $\mu_{ij}(\omega) \neq 1$ generally accepted for describing media with a negative refractive index.

We consider the most general case of a gyrotropic metamaterial whose gyrotropy occurs exclusively because of nanostructurization without an inversion center, while the substances composing the metamaterial are nongyrotropic (and there is no stationary magnetic field). Then, in addition to the effective $\varepsilon_{ij}(\omega)$ and $\mu_{ij}(\omega)$ tensors, it is necessary to introduce local susceptibilities, which correspond to odd terms in the expansion of the total nonlocal dielectric susceptibility in the powers of $\mathbf{k}$ (beginning with the linear term). These additional susceptibilities, which are sometimes referred to as the coefficients of chirality $\chi(\omega)$ and bianisotropy $\beta(\omega)$, correspond to a linear coupling of the magnetic induction $\mathbf{B}$ to the electric field $\mathbf{E}$ and of the electric induction $\mathbf{D}$ to the magnetic field $\mathbf{H}$ [41–44].

It is known that a necessary condition for the existence of such susceptibilities is the absence of both the inversion center and time reversibility [45]. In the case of metal–dielectric metamaterials, the first condition is ensured by the asymmetry of the unit cell, and the second condition is always fulfilled because metals are absorbing media.

As an example, we consider the case of a plane electromagnetic wave (propagating along the $z$ axis) incident normally on a layer of a metamaterial in the plane $xy$. Then, in the most general case of a gyrotropic metamaterial consisting of nongyrotropic components, the effective electromagnetic response can be completely described by introducing *ten* linearly independent coefficients of response in the far field, which relate the tangential components of the fields $(\mathbf{D}_{\|}, \mathbf{B}_{\|})$ to $(\mathbf{E}_{\|}, \mathbf{H}_{\|})$,

$$\begin{pmatrix} D_x \\ D_y \\ B_x \\ B_y \end{pmatrix} = \hat{\eta}_{\|}(\omega, \mathbf{k}_{\|})|_{\mathbf{k}_{\|}=0} \begin{pmatrix} E_x \\ E_y \\ H_x \\ H_y \end{pmatrix}, \tag{1}$$

where

$$\hat{\eta}_{\|} = \begin{pmatrix} \varepsilon_{xx} & \varepsilon_{xy} & \mathrm{i}\chi_x & \mathrm{i}\beta_x \\ \varepsilon_{xy} & \varepsilon_{yy} & -\mathrm{i}\beta_y & -\mathrm{i}\chi_y \\ -\mathrm{i}\chi_x & \mathrm{i}\beta_y & \mu_{xx} & \mu_{xy} \\ -\mathrm{i}\beta_x & \mathrm{i}\chi_y & \mu_{xy} & \mu_{yy} \end{pmatrix}. \tag{2}$$

The ten components $\varepsilon_{xx}$, $\varepsilon_{yy}$, $\varepsilon_{xy}$, $\mu_{xx}$, $\mu_{yy}$, $\mu_{xy}$, $\beta_x$, $\beta_y$, $\chi_x$, and $\chi_y$ (for the normal incidence of light) of the effective response of the layer of the metamaterial thus introduced can be obtained [46] by parameterizing the scattering matrix

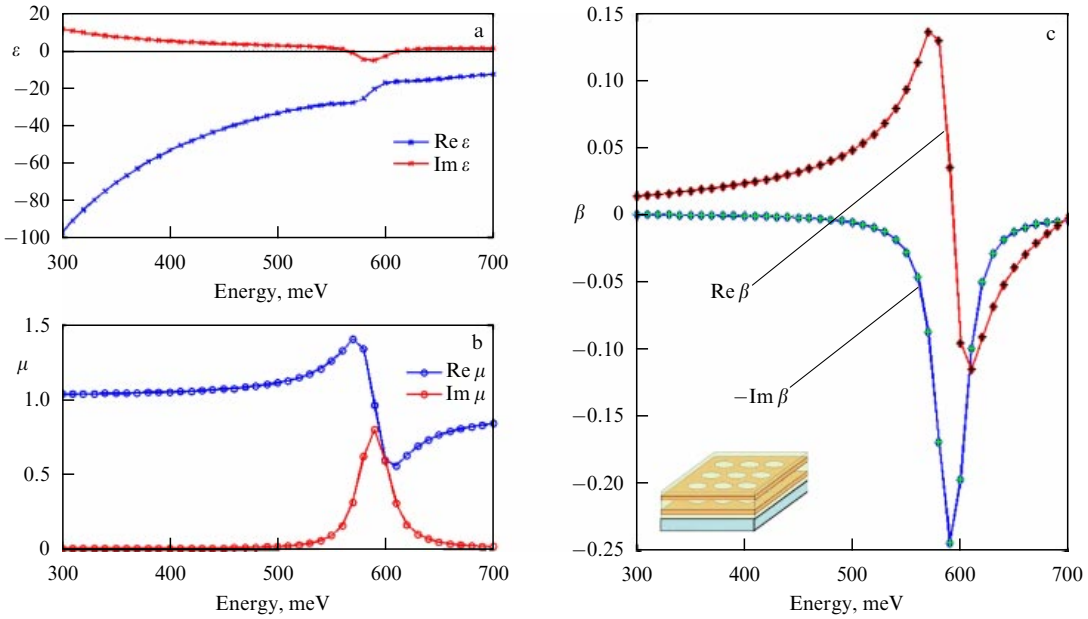


**Figure 1.** Frequency dependence of the effective electromagnetic response coefficients $\varepsilon$, $\mu$, and $\beta$ for a metamaterial layer of the bi-fishnet type [28] on a glass substrate ($\varepsilon = 2.32$). The layers represent gold films 10 nm thick perforated by a square lattice of holes (with the period 838 nm and the diameter of holes 360 nm); the films are separated by a dielectric ($\varepsilon = 2.72$) with the thickness 60 nm.

in the far field calculated for this layer [19, 47, 48]. For the normal incidence of light with the wavelength exceeding the period of the metamaterial (such that there is no diffraction, and the layer of the metamaterial behaves like a layer of a uniform material), the scattering matrix in the far field has the size $4 \times 4$ and is symmetric ($S_{ij} = S_{ji}$) as a result of the reciprocity of the channels of scattering. Therefore, only 10 of the 16 components of $S_{ij}$ are linearly independent, for example, those with $i \leqslant j$, which exactly corresponds to the number of linearly independent response coefficients in formula (1).

The results of the parameterization of the scattering matrix for metamaterials layers of a bi-fishnet type [28] are illustrated in Fig. 1 for an asymmetric dielectric environment and in Fig. 2 for a symmetric environment. A frequency region is shown near the plasmonic magnetic resonance at $\hbar\omega = 0.6$ eV in which the system has a negative refractive index. Although the layer of the metamaterial by itself has an inversion symmetry, it is seen that in the case of an asymmetric dielectric environment, its effective electromagnetic response has a sufficiently strong resonant bianisotropy (Fig. 1c). But if the layer is located in a symmetric dielectric

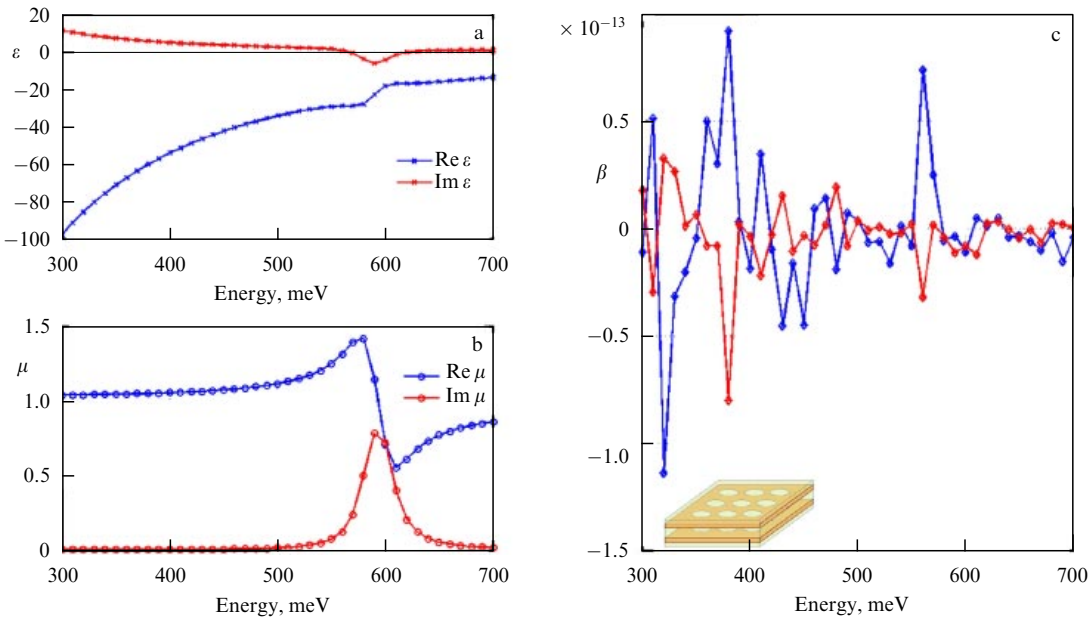


**Figure 2.** Frequency dependence of the effective electromagnetic response coefficients $\varepsilon$, $\mu$, and $\beta$ for a metamaterial layer of the bi-fishnet type analogous to the material described in Fig. 1, but in a symmetric dielectric environment (air from above and from below). The bianisotropy coefficient in this case vanishes, which indicates that the structure as a whole is centrally symmetric.

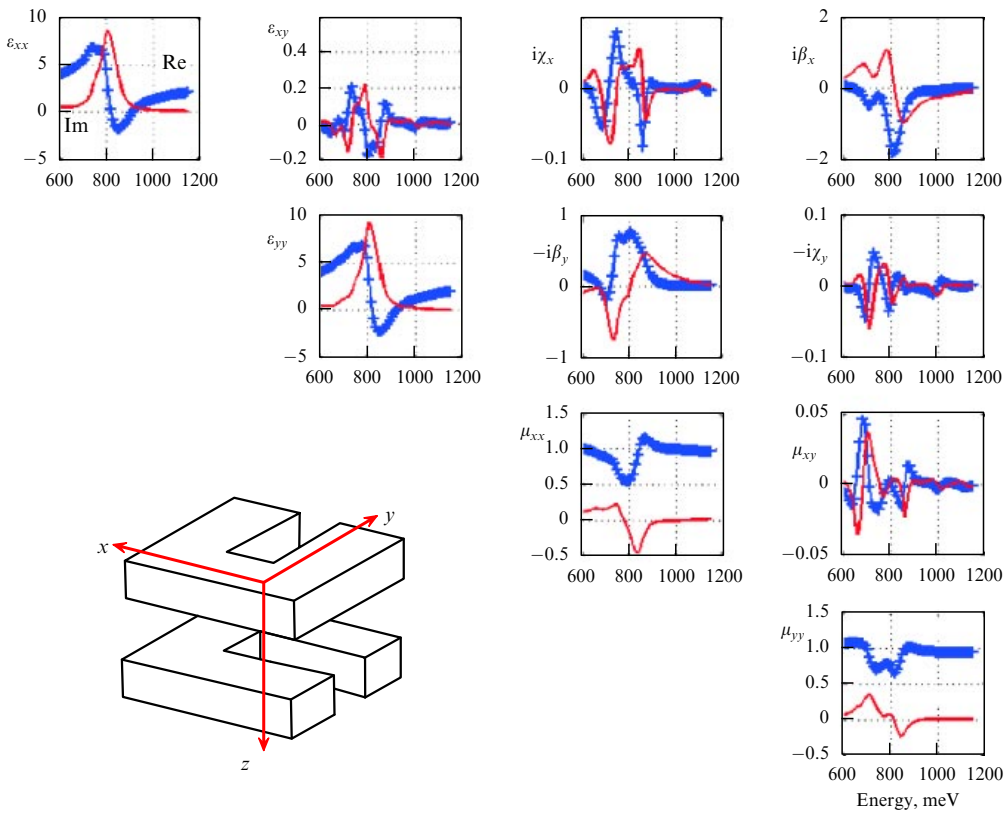


**Figure 3.** Frequency dependence of the effective coefficients of electromagnetic response $\hat{\eta}_{||}$ [see Eqn (1)] for a layer of metamaterial in the form of C resonators turned by an angle of 90°. The solid (blue) curves correspond to the real parts of the coefficients, and the thin lines, to the imaginary parts. The unit cell of the bi-layer is shown in the inset. The horizontal dimensions of a C resonator are $230 \times 230$ nm$^2$, the horizontal width of the line is 90 nm, the thickness is 50 nm, the spacing between the layers of the rotated C resonators is 70 nm. The layer of the metamaterial is obtained as a result of horizontal translations of the unit cell with a square lattice of $700 \times 700$ nm. The C resonators made of gold are located inside the dielectric layer with $\varepsilon = 2.4$ on the surface of glass ($\varepsilon = 2.25$).

environment (see Fig. 2), the bianisotropy disappears, as in the case of a centrally symmetric structure. These results are the direct demonstration of the nonlocality of the electromagnetic response of thin layers of metamaterials: the effective susceptibilities are not only the characteristics of the structure itself but also depend on the dielectric environment. Therefore, the effective susceptibilities can be used only with great caution, remembering that they are not the characteristics of a bulk metamaterial, but adequately characterize only the response of a specific finite-thickness structure in a given dielectric environment.

Figure 3 shows the results of parameterization of the scattering matrix for a thin layer of a chiral stereometamaterial [31], which has strong natural optical activity. In this case, the system has the complete set of nonzero components of the response matrix $\hat{\eta}_{||}$.

**Acknowledgments.** We are grateful to T Ishihara, H Giessen, T Weiss, and A Christ for numerous discussions and cooperation. This work was supported in part by the Russian Foundation for Basic Research, the Presidium of the Russian Academy of Sciences, and the Division of Physical Sciences, Russian Academy of Sciences.

## References

1. Barnes W L , Dereux A, Ebbesen T W *Nature* **424** 824 (2003)
2. Smith D R, Pendry J B, Wiltshire M C K *Science* **305** 788 (2004)
3. Shalaev V M *Nature Photon.* **1** 41 (2007)
4. Klimov V V *Usp. Fiz. Nauk* **178** 875 (2008) [*Phys. Usp.* **51** 839 (2008)]
5. Polman A *Science* **322** 868 (2008)
6. Bykov V P *Zh. Eksp. Teor. Fiz.* **62** 505 (1972) [*Sov. Phys. JETP* **35** 269 (1972)]
7. Zengerle R *J. Mod. Opt.* **34** 1589 (1987)
8. Yablonovitch E *Phys. Rev. Lett.* **58** 2059 (1987)
9. John S *Phys. Rev. Lett.* **58** 2486 (1987)
10. Ivchenko E L, Nezvizhevskii A N, Jorda S *Fiz. Tverd. Tela* **36** 2118 (1994) [*Phys. Solid State* **36** 1156 (1994)]
11. Kochereshko V P et al. *Superlatt. Microstruct.* **15** 471 (1994)
12. Fujita T et al. *Phys. Rev. B* **57** 12428 (1998)
13. Yablonskii A L et al. *J. Phys. Soc. Jpn.* **70** 1137 (2001)
14. Shimada R et al. *IEEE J. Quantum Electron.* **38** 872 (2002)
15. Wood R W *Philos. Mag.* **4** 396 (1902)
16. Fano U *J. Opt. Soc. Am.* **31** 213 (1941)
17. Ebbesen T W et al. *Nature* **391** 667 (1998)
18. Linden S, Kuhl J, Giessen H *Phys. Rev. Lett.* **86** 4688 (2001)
19. Christ A et al. *Phys. Rev. Lett.* **91** 183901 (2003)
20. Teperik T V, Popov V V, García de Abajo F J *Phys. Rev. B* **71** 085408 (2005)
21. Teperik T V et al. *Nature Photon.* **2** 299 (2008)
22. Belotelov V I, Doskolovich L L, Zvezdin A K *Phys. Rev. Lett.* **98** 077401 (2007)
23. Zharov A A, Kurin V V *J. Appl. Phys.* **102** 123514 (2007)
24. Veselago V G *Usp. Fiz. Nauk* **92** 517 (1967) [*Sov. Phys. Usp.* **10** 509 (1968)]
25. Pendry J B *Phys. Rev. Lett.* **85** 3966 (2000)
26. Smith D R et al. *Phys. Rev. Lett.* **84** 4184 (2000)
27. Podolskiy V, Sarychev A, Shalaev V *Opt. Express* **11** 735 (2003)
28. Zhang S et al. *Phys. Rev. Lett.* **95** 137404 (2005)
29. Pendry J B, Schurig D, Smith D R *Science* **312** 1780 (2006)
30. Liu N et al. *Nature Mater.* **7** 31 (2008)
31. Liu N et al. *Nature Photon.* **3** 157 (2009)
32. Valentine J et al. *Nature* **455** 376 (2008)
33. Papakostas A et al. *Phys. Rev. Lett.* **90** 107404 (2003)

34. Kuwata-Gonokami M et al. *Phys. Rev. Lett.* **95** 227401 (2005)
35. Ishihara T, Koshino K, Nakashima H *Phys. Rev. Lett.* **91** 253901 (2003)
36. Hatano T et al. *Phys. Rev. Lett.* , in press (2009); arXiv:0904.4800
37. Agranovich V M, Gartstein Yu N *Usp. Fiz. Nauk* **176** 1051 (2006) [*Phys. Usp.* **49** 1029 (2006)]
38. Simovski C R, Tretyakov S A *Phys. Rev. B* **75** 195111 (2007)
39. Smith D R et al. *Phys. Rev. B* **65** 195104 (2002)
40. Smith D R, Schurig D, Mock J J *Phys. Rev. E* **74** 036604 (2006)
41. Pendry J B *Science* **306** 1353 (2004)
42. Chen X et al. *Phys. Rev. E* **71** 046610 (2005)
43. Rill M S et al. *Nature Mater.* **7** 543 (2008)
44. Kwon D-H et al. *Opt. Express* **16** 11822 (2008)
45. Figotin A, Vitebsky I *Phys. Rev. E* **63** 066609 (2001)
46. Tikhodeev S G, Weiss T, Gippius N A, in preparation (2009)
47. Tikhodeev S G et al. *Phys. Rev. B* **66** 045102 (2002)
48. Gippius N A, Tikhodeev S G, Ishihara T *Phys. Rev. B* **72** 045138 (2005)


PACS numbers: 36.40.Gk, 73.20.Mf, **78.67.–n**
DOI: 10.3367/UFNe.0179.200909i.1007

# Plasmon effects in In(Ga)N-based nanostructures

T V Shubina, S V Ivanov,
A A Toropov, P S Kop'ev

In this report, we consider the influence of effects of localized plasmons in metallic nanoparticles on optical processes in In(Ga)N-based structures. The emission and absorption of light and the generation of photoinduced charge carriers is investigated; data on the estimation of the averaged enhancement in InN/In nanocomposites are given.

Plasmonics is a rapidly developing field of applied physics and nanotechnology characterized by the use of effects related to collective oscillations of conduction electrons in metallic structures (plasmons), frequently for quite uncommon applications [1]. The many-sidedness of plasmonics is manifested in various applications such as the realization of media with a negative refractive index [2], the creation of markers used in decoding human genome [3], the enhancement of the luminescence of organic semiconductors [4], an increase in the efficiency of photodetectors [5] and light-emitting diodes [6], controlling liquid-crystal layers [7], and the generation of emission in the terahertz range [8]. Of great interest are also the fundamental properties of plasmonic metastructures, for example, the formation of strong plasmon–polariton resonances, which can be efficiently controlled by changing their structure [9, 10].

There is one additional promising avenue for the realization of the potential of plasmonics: the creation of single-photon sources that can work at room temperature. The local enhancement of an electromagnetic field by plasmons and, correspondingly, an increase in the rate of spontaneous recombination near a metallic surface are analogs of the Purcell effect [11] in microresonators. We note that a reproducible production of microresonators with quantum dots based on wide-gap semiconductors for the same purpose is at present quite problematic.

Here, we consider optical effects in semiconductor layers and nanocomposites caused by localized plasmons (Mie resonances) excited in metallic nanoparticles. The use of particles instead of a continuous film has some advantages [12]. In particular, because of the curvature of the particle surfaces, the interaction of plasmonic excitation and light emission, forbidden due to a difference in their wave vectors, is then allowed. In essence, the study whose results are presented in this report, especially in the part that concerns nanocomposites, is a continuation of the investigation of InN layers with spontaneously formed In clusters [13–19]. In the course of this investigation, we discovered Mie resonances in the spectra of thermally detected optical absorption (TDOA) and established that the plasmons exert a noticeable influence on the emission. For illustration, Fig. 1 depicts combined images obtained via scanning electron microscopy (SEM) and micro-cathodeluminescence (micro-CL) studies of one and the same region of an InN layer. These images show an enhancement of infrared micro-CL near metallic clusters and near pores surrounded by In precipitates.

Current studies are mainly conducted using two systems: (1) InGaN and an Au nanoparticle, and (2) InN with specially formed In clusters. The choice of these pairs of materials is by no means accidental. The energy of plasmonic resonances in Au particles is close to the energy of excitonic transitions in layers of the solid alloy $In_{0.25}Ga_{0.75}$. Indium as a plasmonic metal is less known than gold. But, the applicability of a metal for the amplification of optical processes is determined by the oscillator strength of plasma resonance. The spectral dependence of this parameter can be described by the ratio of the real part of the complex dielectric function of metal to its imaginary part, $|\mathrm{Re}\,\varepsilon|/\mathrm{Im}\,\varepsilon$. In the infrared range (0.7–1 eV), where radiative optical transitions are observed in InN, this ratio for In is not less than that for Au in the visible range (about 2 eV) (Fig. 2).

An increase in the efficiency of emission implies the formation of coupled localized plasmon–radiating dipole states. For the radiative plasmon decay, the metallic particle can act as a radiating antenna; but in the case of the dominance of a nonradiative decay (with large internal losses of the particle), the coupling can quench emission of the radiating dipole. The balance between these components depends, among other factors, on the particle size [20]. In the general case, to guarantee the interaction of the radiating dipole and localized plasmon, a number of conditions must be

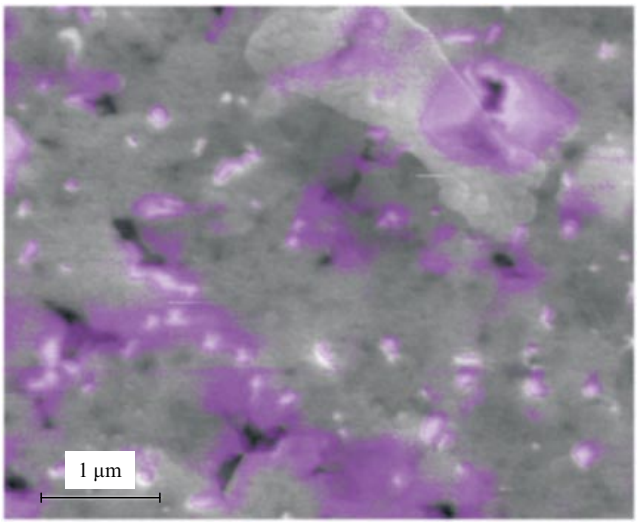


**Figure 1.** Superimposed images of the same region of a layer of InN obtained by SEM and micro-CL. The clusters and pores are respectively seen as bright and dark spots. The violet spots (in the electronic version of the paper at http://www.ufn.ru) correspond to intense infrared (0.75 eV) cathodoluminescence.

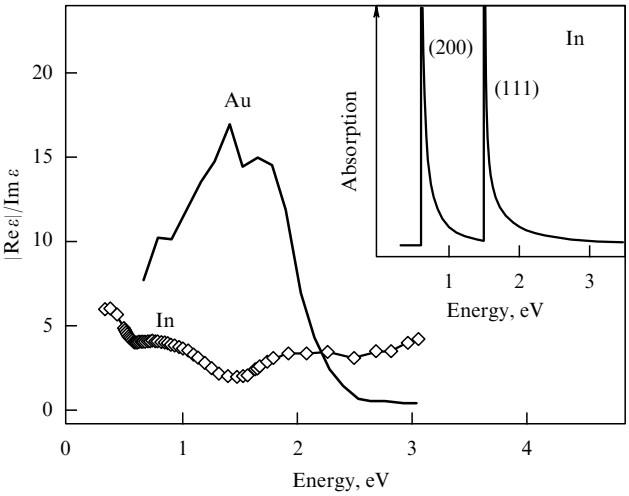


**Figure 2.** $|\mathrm{Re}\,\varepsilon|/\mathrm{Im}\,\varepsilon$ spectra for Au and In. The inset shows the absorption spectrum of In (without taking the electron scattering into account) due to (200) and (111) transitions between parallel bands.

satisfied, such as (1) the spatial proximity of the dipole and metallic particle, (2) the correct orientation of the dipole relative to the direction of the plasmon polarization, and (3) the coincidence of resonance frequencies.

In the approximation of a metallic cluster by an ellipsoid of revolution (spheroid) (with $c$ being the semiaxis of revolution, and the equatorial semiaxes $a$ and $b$ being equal to each other), the frequency $\omega_i$ of the plasmon polarized along the $i$th axis of the spheroid ($i = x, y, z$) is determined by the resonance condition $\varepsilon(\omega) = -\varepsilon_1(L_i^{-1} - 1)$, where $\varepsilon_1(\omega)$ is the permeability of the environment and $L_i$ is the depolarizing factor depending on the ratio of the lengths of the axes. The approximated expression for the frequency is written as [21]

$$\omega_i = \omega_\mathrm{p}\left[\varepsilon_\infty + \varepsilon_1(L_i^{-1} - 1)\right]^{-1/2}, \tag{1}$$

where $\omega_\mathrm{p}$ and $\varepsilon_\infty$ are the plasma frequency and the dielectric constant of the bulk metal. According to Eqn (1), $\omega_i$ depends substantially on the permeability of the environment and on the shape of the cluster. For example, the plasmonic frequency in bulk indium corresponds to 11.2 eV, and in a spherical In cluster located in InN ($\varepsilon_1 \sim 8$), the Mie resonance is at 2.8 eV. Resonances in clusters with the ratio $c/a$ that considerably differs from unity fall into the infrared range if the plasmon is polarized along the longer axis of the spheroid.

In the first approximation, the plasmonic enhancement of luminescence and absorption is proportional to $|g|^2$, where $g = E/E_0$ is defined as the ratio of the local electric field to the field of the incident light wave $E_0$ [22]. With the polarization along the $i$th axis, the partial factor of field enhancement in the vicinity of the $i$th pole of the spheroid is given by

$$|g_i(\omega)| = \left|\frac{\varepsilon(\omega)}{\varepsilon_1(\omega) + L_i\big(\varepsilon(\omega) - \varepsilon_1(\omega)\big)}\right|. \tag{2}$$

At the resonance frequency $\omega_i$, the partial factor $|g_i(\omega)|$ reaches the value $L_i^{-1}|\mathrm{Re}\,\varepsilon|/\mathrm{Im}\,\varepsilon \gg 1$. Generally, the enhancement factor $|g_i(\omega, \mathbf{r})|$ as a function of position $\mathbf{r}$ on the surface of the spheroid varies from the value given by Eqn (2) to the extremely small value $L_i^{-1}|\mathrm{Re}\,\varepsilon_1|/\mathrm{Im}\,\varepsilon \sim 1$ at the pole of an orthogonal axis (not equal to the $i$th axis) [19, 23].

The application of near-field scanning optical microscopy has allowed investigating the interaction of a localized plasmon in a single Au particle with a limited number of excitonic dipole transitions in an InGaN layer [24]. The layers were grown by the method of molecular beam epitaxy (MBE) using a regime that facilitates the formation of a nanocolumnar relief of the surface [25], which was confirmed by the data of transmission electron microscopy (TEM) (Fig. 3a). Fluctuations of the solid alloy composition led to the appearance of deeply localized states, similar to quantum dots [26]. The use of a Nanonics CryoView 2000 microscope allowed simultaneously obtaining maps of the intensity of microphotoluminescence (micro-PL) and a three-dimensional relief of the surface. A gold nanoparticle of a spheroidal shape, from 50 to 200 nm in size, was attached to the tip of a nonaperturate probe. This allowed precisely positioning the particle with respect to the InGaN layer.

The basic result of this experiment was the observation of an enhancement of the emission intensity as the gold particle approached the surface of the InGaN layer (Fig. 3b). In addition, the appearance of narrow lines in the low-temperature spectra, corresponding to the recombination of single excitons, was noted, which is a prerequisite for investigating the InGaN/Au system for the purpose of creating single-photon emitters. We note that the intensity of photoluminescence at room temperature was enhanced by a factor of several tens, whereas the previous studies of single

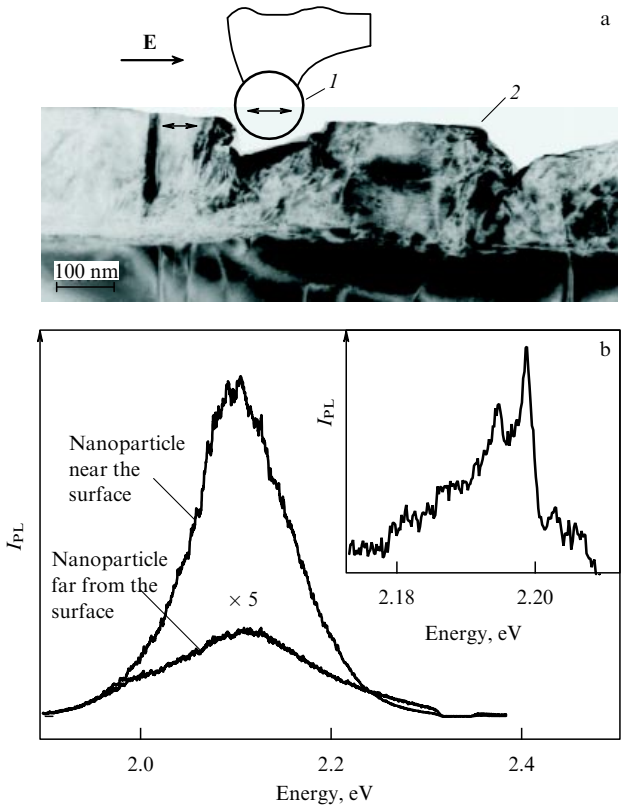


**Figure 3.** (a) A schematic of a probe with an Au nanoparticle (*1*), shown along with a TEM image (*2*) of the transverse section of a layer of InGaN. The left right arrows correspond to the orientation of the dipole in the layer and to the polarization of the plasmon in the particle for case of effective enhancement. (b) Micro-CL spectra measured for the cases where the Au nanoparticle is located near and far from the layer surface (at $T \approx 300$ K). The inset show narrow lines of excitonic photoluminescence in the low-temperature spectrum ($T = 12$ K).

molecules of organic dyes and colloidal quantum dots showed only a moderate (up to a few times) enhancement [27, 28]. Possibly, one of the reasons for this difference is the roughness of the samples being investigated. A comparison of the maps of photoluminescence intensity with images obtained by atomic force microscopy registered for the same region showed that the brightest spots of photoluminescence typically corresponded to dips in the relief into which the tip of the probe could sink. We note that according to electrodynamics, precisely in such a configuration the plasmon in the metallic particle polarized along the electric field vector can efficiently interact with the dipole of the exciton in the case of confocal optical microscopy. We also note that the enhancement observed for Au particles with the diameter 100 nm was absent for particles with the diameter 50 nm. This agrees well with the estimation using the model in [29]. The critical size of the spherical Au particle that allows enhancement is close to 100 nm.

Studying InN/In nanocomposites allowed understanding the specific features of the action of plasmonic resonances on the basic optical processes (emission, absorption, generation of carriers by light) in the case where the metallic clusters are located inside an optically active semiconductor matrix. The most distinct results followed from the analysis of a series of structures with periodic In inserts grown by the MBE method [23]. The inserts (6 or 20 in number) had a nominal thickness from 2 to 48 monolayers (MLs); the thickness of an ML is of the order of 0.3 nm. The inserts were separated by InN layers with the thickness 25 nm, which was grown using the ratio of the flux of N to the flux of In slightly exceeding unity for the purpose of suppressing spontaneous formation of In clusters. However, the TEM data indicate that the In clusters are formed even under these conditions.

Studies of samples by the micro-CL method were conducted using a Hitachi S4300SE microscope equipped with a detector with the sensitivity threshold 0.6 eV. The critical thickness of the metallic inserts of In in InN is $\sim 1$ ML. If this thickness is exceeded, the flat inserts are transformed into arrays of clusters. There then occur processes of a coarsening of the clusters and their accumulation near defects with the formation of agglomerates. These agglomerates are clearly seen in SEM images as brighter regions (Fig. 4). In the sample without inserts, no visible agglomeration of clusters exists, and the CL is weak and almost uniform. The bright spots of CL always coincide with the accumulations of clusters of In. A study in the so-called spot regime of a sample with inserts 48 MLs in thickness showed that the intensity of emission at the agglomerations of the In clusters exceeds the intensity of the signal from the regions between them by a factor of 70. On the average, this sample demonstrates emission that is five times brighter than that of the layer without inserts.

In real nanocomposites, the clusters can have an arbitrary shape and orientation relative to the electric field vector. To estimate the enhancement averaged over an ensemble of clusters, we considered a model of spheroids with a random ratio of semiaxes $a/c$, which had an equal (unit) volume [23]. The inhomogeneously broadened enhancement spectrum $G(\omega) = \langle |g(\omega, \mathbf{r})|^2 \rangle$, determined by the full set of plasmons, was obtained by averaging over the shape of clusters specified by the axial ratio $a/c$. The variation of the relation between the areas of regions with small and large surface curvatures and the depth of penetration of the field into the semiconductor were also taken cuto account. The electronic structure of

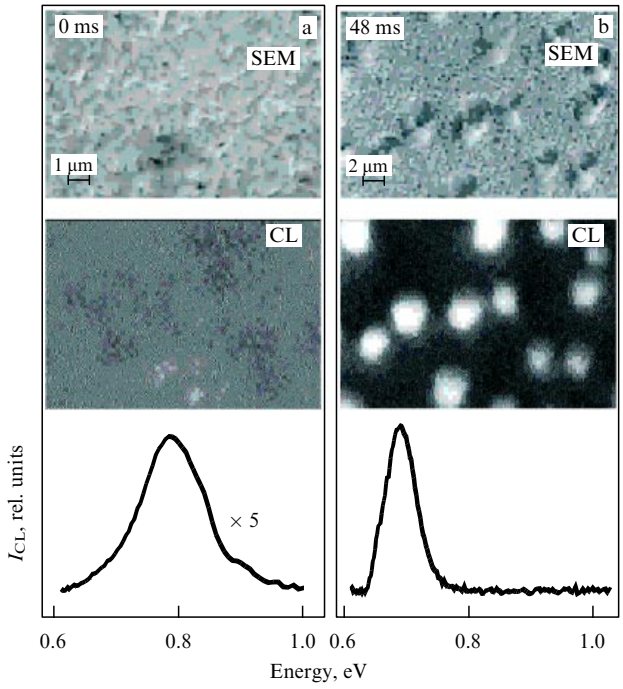


**Figure 4.** Comparison of an SEM image, a micro-CL pattern, and emission spectra obtained from the same region of two structures: (a) without metallic inserts; and (b) with In inserts (48 MLs thick). The bright emission spots coincide with agglomerates of In clusters.

indium is characterized by the presence of parallel regions of electron bands, between which intense transitions near the Fermi surface are possible, leading to an additional absorption in the infrared range (the (111) and (200) transitions in Fig. 2 are denoted in accordance with the classification in [30]). This feature was also taken into account in the calculations.

The maximum value of the emission and absorption enhancement coefficient $|g(\omega_i)|^2$ for an elementary plasma excitation in InN/In, according to Eqn (2), is equal to $10^3 - 10^4$ in surface regions with a large curvature. But because of the small fraction of such regions and a dispersion in the shape of the spheroids, the average enhancement in the nanocomposites does not exceed $10^2$ at the energy 0.7 eV for the distribution center position $a/c = 1$ (sphere) and the distribution width $\delta < 10$. The averaged value of enhancement obtained agrees well with the data on the enhancement of micro-CL near clusters. The spectral dependences in Fig. 5 show that an increase in $\delta$ must shift the main peak in the absorption spectra into the region of lower energies and sharpen its edge, because the elementary resonances are strongest in this region. A comparison of Figs 5a and 5b illustrates the suppression of plasmonic enhancement by interband transitions in the semiconductor matrix, as was noted in [14]. The same effect comes from the transitions between parallel bands in In. This, in particular, causes the dip frequently observed in TDOA spectra [15–17] at the energy 1.5 eV, which corresponds to (111) transitions.

Metal–semiconductor nanocomposites are extremely inhomogeneous media. It can be assumed that some optical processes in them can occur in different regions, which are under different plasmon influences. The most distinct results that confirm this were obtained by a comparison of the spectra of TDOA and photocurrent in InN/In. The ther-

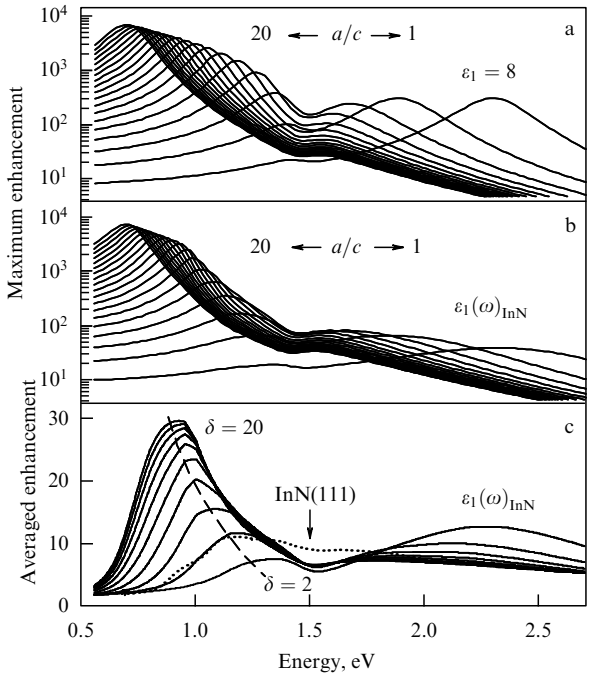


**Figure 5.** Spectra of maximum enhancement at various values of the axial ratio $a/c$ (the range and the direction of the variation of $a/c$ are shown in the figure): (a) matrix without absorption ($\varepsilon_1 = 8$); (b) matrix with absorption (energy gap $E_g \sim 1$ eV); (c) averaged spectra of enhancement calculated for various values of ($E_g \sim 1$ eV). Good agreement is observed between the calculated spectrum ($\beta = 4$) and experimental TDOA spectrum (dashed line) for the sample with a layer 48 MLs thick.

mally detected absorption technique records an increase in the sample temperature, which can be caused by two factors: interband absorption in the matrix and a dissipative decay of plasmons in metallic clusters. On the other hand, the generation of charge carriers under optical excitation arises only in the interband absorption region in InN. Therefore, the difference in the TDOA and photocurrent spectra indicates the existence of plasmonic resonances.

The photocurrent spectra were recorded under excitation by semiconductor lasers with the power 100 mW at various wavelengths. Under excitation by an incandescent lamp, the signal in the absorption edge region was negligible, in contrast to signals in other semiconductors, e.g., GaN and GaAs, in which a photocurrent can easily be excited by the lamp light in the same experimental configuration. The edges of the absorption and photocurrent spectra in these compounds were virtually coincident. But in nanocomposites, the edge of the TDOA proved to be substantially lower than the photocurrent-related edge (Fig. 6a), which can be explained by the contribution of optical losses due to a dissipative decay of plasmonic resonances. We emphasize that plasmons could enhance the rate of generation of charge carriers that form the photocurrent [31] if some density of states existed in this region. Consequently, the matrix indeed has an absorption edge shifted to the region of high energies, which can be partly caused by deviations from the stoichiometry that accompany the formation of clusters [32, 33].

At present, there is great interest in InN as a promising material for solar cells [34]. Based on the data obtained, it can be concluded that the absence of real achievements in this area is possibly connected with the neglect of spontaneous formation of In clusters. On the one hand, the plasmons in these clusters enhance photoluminescence, but on the other hand, the effective absorption edge of the matrix is shifted toward higher energies in such structures and the density of defects is increased [35]. This suppresses the photovoltaic response in InN at excitation energies less than 1.3–1.5 eV.

In InN/In nanocomposites, terahertz emission (with a frequency about 3 THz) was registered upon pumping by electric pulses [36, 37]. The measurements were conducted at the temperature 4.2 K, as was described in [38]. The nature of the terahertz emission is being refined at present. It has been reliably established that its intensity depends on the concentration $n$ of free electrons and mobility $\mu$ (Fig. 6b). The

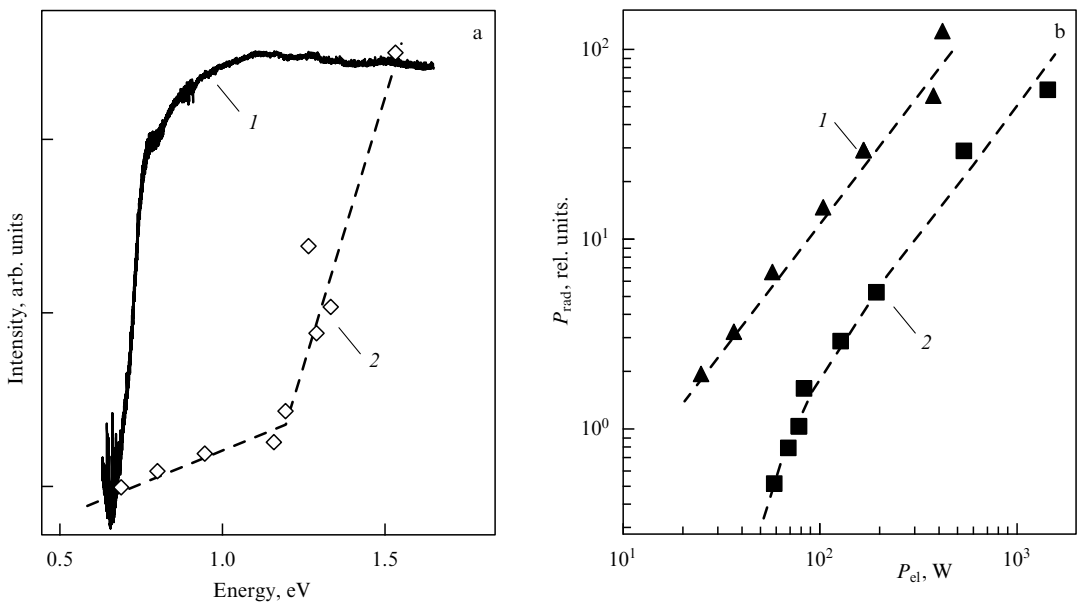


**Figure 6.** (a) TDOA spectra (curve *1*) and photocurrent spectra (curve *2*) in a nanocomposite InN/In. (b) The dependence of the power of terahertz emission ($\sim 3$ THz) on the pumping power in structures with the following parameters: (*1*) $n = 5 \times 10^{18}$ cm$^{-3}$, $\mu = 1000$ cm$^2$ V$^{-1}$ s$^{-1}$; and (*2*) $n = 1 \times 10^{19}$ cm$^{-3}$, $\mu = 200$ cm$^2$ V$^{-1}$ s$^{-1}$.

emission spectral range agrees with the terahertz emission mechanism due to two-dimensional plasmons excited in the semiconductor matrix of the *n* type [39]. In this case, the observed increase in the intensity of terahertz emission with increasing the power of pumping can be related to an increase in the temperature of the electron gas, which facilitates thermal filling of plasmonic modes [40]. SEM studies with a subsequent Fourier transformation of images showed that the nanocomposites frequently exhibit a periodicity in the arrangement of nanocolumns, clusters, and pores. The fulfillment of the condition for the Bragg diffraction on structural inhomogeneities can favor an effective generation of terahertz emission. At the same time, the radiative decay of localized plasmons in sufficiently large In clusters has characteristic times corresponding to close frequencies that can indicate the involvement of these plasmons in the emission generation process.

We have considered effects related to the excitation of localized plasmons in metallic nanoparticles and their interaction with dipole transitions in a semiconductor. Experimental results are given for systems based on In(Ga)N. However, preliminary studies show that similar results can also be obtained for other semiconductors. This opens up great possibilities for the application of plasmonic effects in optoelectronics.

**Acknowledgments.** We are grateful to the researchers who took part in this work, in particular, to N A Gippius, V A Shalygin, V A Kosobukin, and T A Komisarova. This work was supported in part by the Russian Foundation for Basic Research (project Nos 07-02-00786a and 09-02-01305a) and by the Presidium of the Russian Academy of Sciences (program No. 27).

## References

1. Ozbay E *Science* **311** 189 (2006)
2. Shalaev V M *Nature Photon.* **1** 41 (2007)
3. Wabuyele M B, Vo-Dinh T *Anal. Chem.* **77** 7810 (2005)
4. Bellessa J et al. *Phys. Rev. Lett.* **93** 036404 (2004)
5. Hetterich J et al. *IEEE J. Quantum Electron.* **43** 855 (2007)
6. Shen K-C et al. *Appl. Phys. Lett.* **93** 231111 (2008)
7. Kamaga C et al. *Appl. Phys. Lett.* **91** 173119 (2007)
8. Chen H-T et al. *Nature* **444** 597 (2006)
9. Christ A et al. *Phys. Rev. Lett.* **91** 183901 (2003)
10. Christ A et al. *Nano Lett.* **8** 2171 (2008)
11. Purcell E M *Phys. Rev. B* **69** 681 (1946)
12. Klimov V V *Usp. Fiz. Nauk* **178** 875 (2008) [*Phys. Usp.* **51** 839 (2008)]
13. Shubina T V et al. *Phys. Rev. Lett.* **92** 117407 (2004); **95** 209901 (2005)
14. Shubina T V et al. *Phys. Rev. Lett.* **93** 269702 (2004)
15. Shubina T V et al. *Phys. Status Solidi A* **202** 2633 (2005)
16. Shubina T V et al. *Phys. Status Solidi A* **203** 13 (2006)
17. Shubina T V et al. *J. Cryst. Growth* **288** 230 (2006)
18. Bartel T P et al. *Appl. Phys. Lett.* **91** 101908 (2007)
19. Shubina T V et al. *Phys. Status Solidi C* **4** 2445 (2007)
20. Crowell J, Ritchie R H *Phys. Rev.* **172** 436 (1968)
21. Kreibig U, Vollmer M *Optical Properties of Metal Clusters* (Berlin: Springer, 1995)
22. Moskovits M *Rev. Mod. Phys.* **57** 783 (1985)
23. Shubina T V et al. *Phys. Rev. B* **79** 153105 (2009)
24. Toropov A A et al. *Phys. Rev. Lett.* **103** 037403 (2009)
25. Jmerik V N et al. *J. Cryst. Growth* **301–302** 469 (2007)
26. Ivanov S V et al. *J. Cryst. Growth* **301–302** 465 (2007)
27. Lakowicz J R *Anal. Biochem.* **298** 1 (2001)
28. Farahani J N et al. *Phys. Rev. Lett.* **95** 017402 (2005)
29. Gersten J, Nitzan A *J. Chem. Phys.* **75** 1139 (1981)
30. Golovashkin A I et al. *Zh. Eksp. Teor. Fiz.* **51** 1623 (1966) [*Sov. Phys. JETP* **24** 1093 (1967)]
31. Westphalen M et al. *Solar Energy Mater. Solar Cells* **61** 97 (2000)
32. Shubina T V et al. *Phys. Status Solidi A* **202** 377 (2005)
33. Shubina T V et al. *Phys. Status Solidi C* **4** 2474 (2007)
34. Wu J et al. *J. Appl. Phys.* **94** 6477 (2003)
35. Komissarova T A et al. *Fiz. Tekh. Poluprov.* **43** 304 (2009) [*Semicond.* **43** 285 (2009)]
36. Shubina T V et al., in *Trudy 1-go Mezhdunar. Foruma po Nanotekhnologiyam, Moskva, 3–5 Dekabrya 2008* (Proc. 1st Int. Forum on Nanotechnologies) (Moscow: Rusnanotekh, 2008) p. 183
37. Shubina T V et al. *Izv. Ross. Akad. Nauk, Ser. Fiz.* **74** 68 (2010)
38. Shalygin V A et al. *Appl. Phys. Lett.* **90** 161128 (2007)
39. Mikhailov S A *SPIE Proc.* **3828** 139 (1999)
40. Höpfel R A, Vass E, Gornik E *Phys. Rev. Lett.* **49** 1667 (1982)

PACS numbers: 42.25.Fx, 78.20.Ls, **78.67.–n**
DOI: 10.3367/UFNe.0179.200909j.1012

# Resonance scattering of light in nanostructured metallic and ferromagnetic films

V V Kurin

## 1. Introduction

In this report, we show that magnetooptical effects can be considerably enhanced in composite nanostructured metamaterials and ferromagnetic photonic crystals. The factors responsible for the enhancement can be both individual resonances in nanoparticles (plasma or geometrical) and collective resonances caused by multiple-scattering effects in lattices of nanoinhomogeneities.

Magnetooptical effects, which consist of a change in light polarization upon interaction with ferromagnetic materials, have been intensely studied for a sufficiently long time and are used in practice for the magnetooptical recording of information [1].

It seems obvious that magnetooptical effects can be substantially enhanced in nanostructured composite materials due to electrodynamic resonance effects, which have been given increased attention recently [2]. The nature of resonances can be different. In particular, these can be resonances connected with the excitation of natural modes of individual nanoinhomogeneities. An example of an enhancement of magnetooptical effects caused by individual resonances in a medium consisting of ferromagnetic nanospheres was first considered in Ref. [3].

Here, we demonstrate that an enhancement of magnetooptical effects can also be caused by resonance effects of another nature, such as the excitation of slowed-down waveguide modes, resonance scattering by nanowaveguides, and multiple scattering effects.

To demonstrate the effects of resonance enhancement of magnetooptical effects, we consider a simple model of an artificial medium consisting of a ferromagnetic film with cylindrical holes, assuming that the magnetization vector is directed along the normal to the film and the sizes of inhomogeneities are less than both the wavelength and the skin depth in the metal. Figure 1 shows a schematic of the scattering of an electromagnetic wave by such a structure and the basic excited waves.

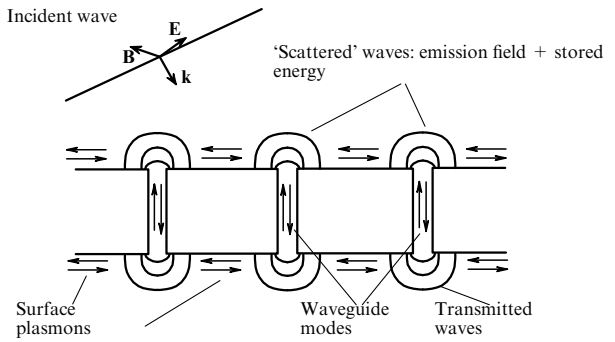


**Figure 1.** Scattering of an electromagnetic wave by a perforated ferromagnetic film (schematic). The main types of waves excited in the process of scattering are shown.

In the visible frequency range, the gyrotropy of a ferromagnet is connected with a gyroelectric mechanism [1] caused by the spin–orbital interaction [4], which manifests itself only in the off-diagonal elements of the dielectric constant tensor. The magnetic permeability can be set equal to the unit diagonal tensor $\mu_{ik} = \delta_{ik}$. In the coordinate system where the $z$ axis is oriented along the magnetization vector $\mathbf{M}$ and the vector $\mathbf{r}_\perp = (x, y)$ lies in the perpendicular plane, the dielectric constant tensor of the ferromagnetic film is analogous in structure to the tensor of the electron gas in a magnetic field and is written in the form

$$\hat{\varepsilon} = \begin{pmatrix} \varepsilon & \mathrm{i}g & 0 \\ -\mathrm{i}g & \varepsilon & 0 \\ 0 & 0 & \eta \end{pmatrix}, \tag{1}$$

where $\varepsilon$ and $\eta$ are respectively the longitudinal and transverse dielectric constants and $g$ is the gyrotropy parameter proportional to the magnitude of the magnetization. A characteristic magnitude of gyrotropy of a typical ferromagnet Co is $g \sim 10^{-2}$, which corresponds to the effective magnetic field $10^6$ G. The diagonal elements of the tensor $\varepsilon \approx \eta \sim 1$ have an order of magnitude characteristic of metals.

## 2. Propagation of waves in a ferromagnetic nanowaveguide

It is natural to begin solving the problem of scattering by a perforated film by studying eigenmodes of a cylindrical nanohole. We assume that the magnetization vector is parallel to the waveguide axis, which is directed along the normal to the film. We note that such a direction of magnetization in a continuous film is sufficiently difficult to realize in view of the large contribution of the magnetostatic energy; therefore, to achieve the vertical magnetization, ferromagnets with a large internal anisotropy must be used. It is known, for example, that such a direction of $\mathbf{M}$ can be realized in films of CoPt and CoPd [5, 6]. But we note that the magnetic state of the film can change because of the presence of openings in the film, because the fields in the openings make a contribution to the free energy of the magnet, and the magnetic state of a film with nanoinhomogeneities must be determined with the aid of micromagnetic calculations.

We consider the problem of eigenwaves of a nanowaveguide in a ferromagnet with the magnetization along the waveguide axis. By finding solutions of the Maxwell equations in the form $(\mathbf{E}, \mathbf{B}) \sim (\mathbf{e}, \mathbf{b}) \times \exp(\mathrm{i}\omega t + \mathrm{i}m\varphi + \mathrm{i}hz)$, where $\omega$ is the frequency, $m$ is the azimuthal index, and $h$ is the longitudinal wave number, and by matching the solutions for the external and internal regions according to the requirement of the continuity of the tangential $(z, \varphi)$ component of the fields, we obtain a dispersion relation, which in the case of weak gyrotropy takes the form

$$\begin{aligned} &\left[\varepsilon_\mathrm{i} f(x) - \eta F(y)\right]\left[f(x) - F(y)\right] - \frac{m^2\zeta^2}{u^2}\left(\frac{1}{x^2} + \frac{1}{y^2}\right)^2 \\ &\quad = \frac{gm}{y^4x^2}\left[\left(2\zeta^2 + x^2\right)\left(x^2 f(x) + y^2 F(y)\right)\right. \\ &\quad \left. + \zeta^2(x^2 + y^2)\frac{\partial y^2 F(y)}{y\,\partial y}\right]. \end{aligned} \tag{2}$$

Here, we let $\varepsilon_\mathrm{i}$ denote the dielectric constant inside the waveguide and introduce dimensionless transverse wave numbers $x = q_\mathrm{i}a$ and $y = \mathrm{i}q_\mathrm{e}a$ (where $q_\mathrm{i}$ and $q_\mathrm{e}$ are the transverse wave numbers for the internal and external regions), dimensionless longitudinal wave number $\zeta = ha$ and frequency $u = ka$, a dimensionless plasma frequency $v = \omega_\mathrm{p}a/c$, and $\eta = 1 - v^2/u^2$, where $a$ is the nanowaveguide radius and $k = \omega/c$ is the wave number in the vacuum; $f(x) = J'_m(x)/\left(xJ_m(x)\right)$ and $F(y) = -K'_m(y)/\left(yK_m(y)\right)$, where $J_m$ and $K_m$ are the respective Bessel and MacDonald functions.

The vanishing of the left-hand side of Eqn (2) yields a well-known dispersion relation for a waveguide in an isotropic nonferromagnetic metal; the right-hand side expresses first-order corrections in $g$ due to gyrotropy, which lift the degeneracy in the azimuthal index $m$. An incident plane wave can excite only waves with $m = \pm 1$; we analyze these waves in the case of narrow channels, where $x$, $y \ll 1$. Expressing the frequency $x$, $y \ll 1$, the longitudinal wave number $u$, and the permeability $\zeta$ in terms of the transverse wave numbers and using the undisturbed dispersion relations $\zeta^2(\varepsilon_\mathrm{i} - 1)^{-1}(\varepsilon_\mathrm{i}x^2 + y^2 - \varepsilon_\mathrm{i}v^2)$, $u^2 = (\varepsilon_\mathrm{i} - 1)^{-1}(x^2 + y^2 - v^2)$, we obtain a closed equation for $x$ and $y$, which is solved explicitly using the expansions $f = x^{-2} - 0.25$ and $F = y^{-2} + \ln 2(\gamma y)^{-1}$ that are valid in the limit of a narrow waveguide and a small gyrotropy parameter $g$. The characteristic dispersion curves are shown in Fig. 2.

As $h \to 0$, the frequencies of modes with the azimuthal indices $m = \pm 1$ tend to the frequency of the surface plasmon $\omega_\mathrm{sp} = \omega_\mathrm{p}(1 + \varepsilon_\mathrm{i})^{-1/2}$, irrespective of the size of the holes. This corresponds to the well-known fact that even an arbitrarily narrow waveguide in a real metal can carry a dipole mode.

We now consider a change in the polarization with the propagation of a wave in the waveguide. For this, we assume

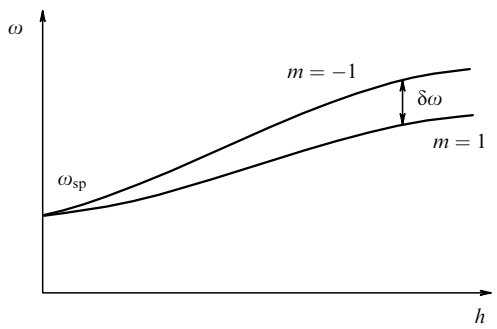


**Figure 2.** Dispersion curves of dipole waveguide modes in a ferromagnetic nanowaveguide.

that the direction of polarization of the waveguide mode is the direction of the electric field vector at the waveguide axis. In the case of a small gyrotropy parameter $g$, we can use the correct zero-approximation eigenvectors and find that the polarization rotation angle, which is given by

$$\theta = \big(h_1(\omega) - h_{-1}(\omega)\big)\, d \approx \frac{\delta\omega\, d}{v_{\mathrm{g}}}\,,$$

is anomalously large as a result of a strong slowdown of waves in the nanowaveguide. Here, $h_{\pm 1}$ are the longitudinal wave numbers of waves with the azimuthal indices $m = \pm 1$, $d$ is the thickness of the ferromagnetic film, $\delta\omega$ is the splitting of dispersion curves with $m = \pm 1$, and $v_{\mathrm{g}}$ is the group velocity. We note that the wave slowdown increases not only the rate of Faraday rotation but also the damping of the waveguide modes. The characteristic attenuation length of the waveguide modes depends on the diameter of the waveguide, and is approximately 10 μm for the diameter of the order of 50 nm.

## 3. Individual resonance in the case of scattering by a single waveguide

In this section, we consider the problem of the transmission and reflection of external electromagnetic radiation upon interaction with a single nanowaveguide in a ferromagnetic film. As previously, we assume that the magnetization is perpendicular to the surface of the film. To solve the problem, we must estimate the efficiency of the excitation of waveguide modes by a wave incident on the upper boundary and the excitation of the transmitted and reflected waves by the arising waveguide modes. The problem can be solved approximately as follows. It is well known [7, 8] that a hole in the metal can be replaced by effective electric and magnetic currents concentrated on both sides of the film in a region with the thickness of the order of the skin depth in the metal, as is shown in Fig. 3.

Near the ends of the waveguide, we separate regions with the depth and the radius of the order of the skin depth in the surrounding metal, in which the effective magnetic and electric currents flow [4], and assume that their multipole moments are known; hence, we find the external fields with respect to these regions. In the free space before the film, this is a set of the fields of multipoles, incident wave, and the wave reflected from the flat surface; in the waveguide, these are only the fields of the counterpropagating waves; in the space on the other side of the film, these are only the fields of the multipoles. We must also write a solution for the internal regions of the ends of the waveguide. The next step consists in matching the tangential components of the internal and external representations of the fields on the surface that separates these regions, and finding the amplitudes of an infinite number of modes in the waveguide, including the nonpropagating ones, as well as of the magnitudes of all multipole moments and the distribution of the field in the vicinities of the waveguide ends.

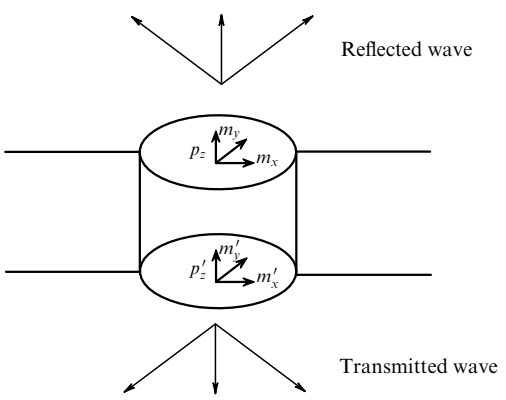


**Figure 3.** Response of a nanowaveguide to external radiation. Effective dipole moments.

If such a procedure were carried out, we would obtain an exact solution of the problem. Unfortunately, this solution leads to complex integral equations, which can be solved only numerically. However, for nanowaveguides with a diameter that is small compared with the wavelength and the skin depth, we can obtain an approximate solution by restricting ourselves to only fields of dipoles outside the nanowaveguide and to only propagating waves inside it. For simplicity, we neglect the intermediate region and match the components of the solution $\mathbf{E}_\perp$ and $\mathbf{B}_\perp$ at one point, e.g., the point on the $z$ axis located at a distance equal to the waveguide radius from the film plane. In this approach, we ignore effects connected with the existence of plasma resonance at the frequency of the surface plasmon $\omega_{\mathrm{sp}}$, assuming that the wave frequency is far from it.

We consider the case of normal incidence, where the scattering occurs only in the magnetodipole channel and the magnetic dipoles have only components that are perpendicular to the $z$ axis. We assume that the incident wave is linearly polarized along the $x$ axis. We decompose the $(\mathbf{E}, \mathbf{B})_\perp$ fields on the $z$ axis and the magnetic dipole moments on one side and the other side of the film $\mathbf{M}^{\mathrm{L}}$ and $\mathbf{M}^{\mathrm{R}}$ into the left-handed and right-handed components $(E, B, M)_\pm = (E, B, M)_x \pm \mathrm{i}(E, B, M)_y$, which are eigenvectors for the field both outside and inside the waveguide; for the field on the side of the wave incidence (L), we then write these components as

$$E_\pm = \exp(\mathrm{i}kz) - \exp(-\mathrm{i}kz) \pm kM_\pm^{\mathrm{L}}(\mathrm{i}k - |z|^{-1})\,\frac{\exp(\mathrm{i}k|z|)}{|z|}\,,$$

$$B_\pm = \pm\mathrm{i}\big[\exp(\mathrm{i}kz) + \exp(-\mathrm{i}kz)\big] + M_\pm^{\mathrm{L}}(k^2 + \mathrm{i}k|z|^{-1} - z^{-2})\,\frac{\exp(\mathrm{i}k|z|)}{|z|}\,;$$

next, for the field on the waveguide axis,

$$E_\pm = c_\pm \exp(\mathrm{i}k_\pm z) + d_\pm \exp(-\mathrm{i}k_\pm z)\,,$$

$$B_\pm = \pm\mathrm{i}\,\frac{k_\pm}{k}\,\big[c_\pm \exp(\mathrm{i}k_\pm z) + d_\pm \exp(-\mathrm{i}k_\pm z)\big]\,,$$

where $k_\pm$ is the solution of dispersion equation (2), and for the transmitted field (R),

$$E_\pm = \mp kM_\pm^{\mathrm{R}}\big(\mathrm{i}k - |z|^{-1}\big)\,\frac{\exp(\mathrm{i}k|z|)}{|z|}\,,$$

$$B_\pm = M_\pm^{\mathrm{R}}\big(k^2 + \mathrm{i}k|z|^{-1} - z^{-2}\big)\,\frac{\exp(\mathrm{i}k|z|)}{|z|}\,.$$

In the last two expressions, the coordinate $z$ is referenced to the right end of the waveguide. In all the expressions, we omit the common factor $\exp(-\mathrm{i}\omega t + \mathrm{i}m\varphi)$, and in the expression for the reflected wave, we neglect the difference from $-1$ for

the reflection coefficient from the metal and ignore the change in the polarization. These simple effects can be easily taken into account, if necessary, in the framework of the suggested scheme. Furthermore, in calculating fields of the dipoles, we disregarded the excitation of a surface plasmon. By matching the solutions, we obtain the magnitudes of the magnetic dipole moments on the left-hand and right-hand boundaries of the nanowaveguide and the amplitudes of the modes propagating in the waveguide. The expression for the magnetic moments on the left-hand boundary of the layer is written as

$$M_{\pm}^{\mathrm{L}} = \mp \mathrm{i} \frac{(h_{\pm}/k)\, G^{E} - \mathrm{i} G^{H} \tan(h_{\pm} d)}{(h_{\pm}/k)\, G^{E} G^{H} - (\mathrm{i}/2)\left[(G^{H})^{2} + (h_{\pm}^{2}/k^{2})(G^{E})^{2}\right] \tan(h_{\pm} d)},$$

and that on the right-hand boundary, as

$$M_{\pm}^{\mathrm{R}} = \pm \mathrm{i} \frac{(h_{\pm}/k)\, G^{E} \cos^{-1}(h_{\pm} d)}{(h_{\pm}/k)\, G^{E} G^{H} - (\mathrm{i}/2)\left[(G^{H})^{2} + (h_{\pm}^{2}/k^{2})(G^{E})^{2}\right] \tan(h_{\pm} d)},$$

where $d$ is the film thickness, $k$ is the wave number in the vacuum, and $G^{E}$ and $G^{H}$ are the electric and magnetic components of the magnetodipole Green's function, which are defined as $G^{E} = -\mathrm{i}ka^{-2}(\mathrm{i}ka - 1)\exp(\mathrm{i}ka)$ and $G^{H} = G^{E} - a^{-3}\exp(\mathrm{i}ka)$. These expressions resemble the formulas for the coefficients of reflection of a plane wave from a layer of a dielectric medium and of the transmission through this medium; but we note that, unlike the law of conservation of the energy flux in the case of a layer, the energy flux conservation law in the case under consideration is given by the so-called optical theorem:

$$\mp \mathrm{Re}\, M_{\pm}^{\mathrm{L}} = \frac{1}{3} k^{3} \left(|M_{\pm}^{\mathrm{L}}|^{2} + |M_{\pm}^{\mathrm{R}}|^{2} + Q\right),$$

where $Q$ denotes the losses in the waveguide. The left-hand side of this expression represents the flux lost from the incident and reflected plane waves. The formulas for $M_{\pm}^{\mathrm{L,R}}$ define it as a positive definite quantity. However, the condition that this flux is equal to the sum of dissipated and absorbed fluxes is violated in general because the matching conditions are here satisfied only approximately. Therefore, the expressions obtained are applicable only under the condition of the smallness of radiation losses compared to the dissipation. Given the formulas for $M_{\pm}^{\mathrm{L,R}}$, we can easily find the Cartesian coordinates of the dipole moments $M_x$ and $M_y$.

Figure 4 qualitatively displays the frequency dependence of the polarization parameters for the backward scattering of linearly polarized radiation in the near-resonance region $kd \sim \pi$. The figure shows the dependence of the angle of the inclination of the major axis of the ellipse of polarization of the magnetic dipole moment with respect to the magnetic field direction in the incident wave of polarization ($\tan\theta = \mathrm{Re}(M_x^{\mathrm{L}}/M_y^{\mathrm{L}})$; dashed curve), and the dependence of the ratio of the minor semiaxis of the ellipse of polarization to the major semiaxis, $b \approx \mathrm{Im}(M_x^{\mathrm{L}}/M_y^{\mathrm{L}})$ (solid curve), on the dimensionless frequency $\Omega = u/u_{\mathrm{res}}$ in the vicinity of one of the resonances, whose frequencies are determined by the relations $h_{+1}(u)\, d \approx h_{-1}(u)\, d \approx n\pi d$. Analogous resonance effects are also to be observed in the case of radiation passing through the film. It is seen from the figure that the angle of the inclination of polarization increases substantially as the resonance is approached. For typical film parameters and room temperature, an approximately tenfold resonant enhancement of the magnetooptical effect can be expected in comparison with that in a continuous ferromagnetic film. For cooled samples, the resonances must be even more clearly pronounced. It is interesting to note that the resonance magnetooptical effect under consideration is characterized by a change in the sign of the rotation angle of the polarization plane in the near-resonance region.

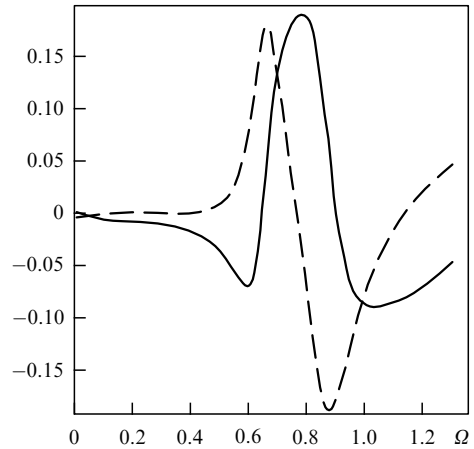


**Figure 4.** Typical frequency dependence of the parameters of the ellipse of polarization of reflected light in the vicinity of one of the resonances with a mode of a finite waveguide. The solid curve shows the ratio of the major axes of the ellipse of polarization of the magnetic dipole moment; the dashed curve demonstrates the behavior of the angle of rotation of its major axis with respect to the polarization direction in the incident wave.

## 4. Multiple scattering effects

If we now consider a lattice of waveguides instead of one nanowaveguide, then the external electromagnetic field in the vicinity of the waveguide ends is determined not only by the fields of waves incident on the metal surface and reflected from it but also by the fields created by effective sources located at the ends of other nanowaveguides.

In the case of a regular lattice, the interaction of individual nanoinhomogeneities is resonantly enhanced when some diffraction maximum becomes grazing, and the diffracted field undergoes a transformation from the field of radiation to the field 'pressed' to the surface. Resonances of this type were discovered experimentally in [9] and were described theoretically in [10]. The experimentally measured resonant enhancement of the local field considerably exceeds the enhancement of the field on single particles, and reach values of the order of several thousand for gold nanoparticles. It is absolutely obvious that these collective resonances, which can naturally be called diffraction resonances, also strongly influence the magnetooptical effects.

The resonance scattering must be described with due care because seemingly natural approximations, which lead to the replacement of an infinite system for the amplitudes of natural waves by a finite system as in Section 3, or, for example, the approximations of a given polarizability described in [8], lead to a violation of the physically natural conservation laws. This restricts the field of the applicability of the formulas obtained to the condition of the domination

of collisional losses over radiative losses. It is obvious that with an increase in the size of the system, the role of collisional losses in the case of diffraction resonance decreases because of an increase in the stored energy, and the requirements concerning the accuracy of the calculations of radiation effects should increase considerably. To achieve physically reasonable results, it is usually necessary to use numerical methods [10]. However, we here describe an example of a problem that allows a self-consistent analytic solution; we also show how it can be extended to the case of a gyrotropic medium.

We consider the simple problem of scattering of a plane electromagnetic wave by a lattice of equispaced (at points $x = 0, y = jL$) narrow parallel cylinders with the generatrices parallel to the $z$ axis. Let the plane of incidence be perpendicular to the generatrices of the cylinders and let the angle of incidence be $\chi$. In this case, the problem splits into two scalar problems, which correspond to two independent polarizations, H and E, with the magnetic and electric field vectors directed along the $z$ axis. We perform calculations for the H polarization, which is more interesting because with this polarization, upon scattering by a cylinder, there exists an individual quasistatic resonance whose frequency is determined from the equation $\varepsilon + 1 = 0$. The calculations for the second polarization are conducted analogously. We write the expressions for the fields outside and inside the cylinders as:

$$B_z^{\text{out}} = \exp(\mathrm{i}k_x x + \mathrm{i}k_y y) + \sum_{m,j} \mathrm{i}^m \exp(\mathrm{i}m\varphi_j)\, D_m^j H_m^1(k\rho_j)\,,$$

$$B^{\text{in}} = \sum_{m,j} \mathrm{i}^m \exp(\mathrm{i}m\varphi_j)\, F_m^j J_m(k\sqrt{\varepsilon}\rho_j)\,, \tag{3}$$

where $D_m^j$ and $F_m^j$ are the multipole coefficients, which respectively characterize the outside and inside fields, $H_m^1(k\rho_j)$ is the Hankel function of the first order, which describes the diverging wave, $J_m(k\rho_j)$ is the Bessel function, and the radius $\rho_j$ is referenced to the center of the $j$th cylinder. Using an expansion of the plane wave in Bessel functions and Graf's addition theorem for the cylinder functions of the shifted argument $\boldsymbol{\rho}_j = \mathbf{x}_0 x + \mathbf{y}_0(y - jL)$, where $L$ is the distance between the cylinders, we represent the external field in the vicinity of the $j$th cylinder as

$$B_z = \sum_m \mathrm{i}^m \exp(\mathrm{i}m\varphi)\Big\{J_m(k\rho_j)\big[\exp(\mathrm{i}kLj\sin\chi - \mathrm{i}m\chi)$$

$$+ \sum_{n,l<j} D_{-n}^l H_{n+m}^1(kL|j-l|)$$

$$+ \sum_{n,l>j} (-1)^{m+n} D_{-n}^l H_{n+m}^1(kL|j-l|)\big] + D_m^j H_m^1(k\rho_j)\Big\}. \tag{4}$$

Thence, it follows that as a result of the emission from cylinders with numbers $l \neq j$, a renormalization of the incident wave occurs. If we now match the external and internal tangential fields $B_z$ and $E_\varphi = \mathrm{i}/(\varepsilon k)\,\partial B_z/\partial\rho$ on the surface of this cylinder, we obtain a set of equations for the multipole coefficients $D_m^j$ and $F_m^j$. In contrast to the procedure used in Section 3, this approach the boundary conditions to be satisfied exactly over the entire surface of the cylinder. This method of solving the problem is an application of the well-known Korringa–Kohn–Rostoker method [11, 12], which was first proposed for scalar quantum mechanical problems and is widely used in calculations of the band structure of solids. (For the extension of this method to vector electrodynamic problems, see [13].) In Ref. [14], an analogous method was used to numerically solve the problem of scattering of an electromagnetic wave by a lattice of isotropic cylinders.

Now, using the translational symmetry of the problem, we perform a discrete Fourier transformation with respect to the order number of cylinders $j$. The formulas for the direct and inverse transformations are determined by the relation

$$D_m^j = \int_{-\pi/L}^{\pi/L} D_m(q) \exp(\mathrm{i}qLj)\, \frac{L\,\mathrm{d}q}{2\pi}\,,$$

$$D_m(q) = \sum_j D_m^j \exp(-\mathrm{i}qLj)\,. \tag{5}$$

The transformation for the incident wave has the form $\delta(qL - kL\sin\chi)\exp(-\mathrm{i}m\chi)$; therefore, by isolating this singularity, $(D_m(q), F_m(q)) = \delta(qL - kL\sin\chi)(D_m, F_m)$, we obtain the following set of equations for the coefficients $(D_m, F_m)$:

$$J_m(ka)\Big[\exp(-\mathrm{i}m\chi) + \sum_n D_{-n} G_{n+m}(kL, \sin\chi)\Big]$$

$$+ D_m H_m^1(ka) = F_m J_m(k\sqrt{\varepsilon}a)\,,$$

$$J_m'(ka)\Big[\exp(-\mathrm{i}m\chi) + \sum_n D_{-n} G_{n+m}(kL, \sin\chi)\Big]$$

$$+ D_m' H_m^1(ka) = \frac{1}{\sqrt{\varepsilon}} F_m J_m'(k\sqrt{\varepsilon}a)\,, \tag{6}$$

which is identical in structure to the set that determines the multipole coefficients in the case of wave scattering by a single cylinder. The only difference is in the additional term in brackets, which describes the renormalization of the incident wave. The coefficients $G_m$ that are responsible for the renormalization are given by

$$G_m(kL, \sin\chi) = \sum_{j>0} H_m^1(kL|j|)$$

$$\times \big[\exp(\mathrm{i}kLj\sin\chi) + (-1)^m \exp(-\mathrm{i}kLj\sin\chi)\big]\,.$$

If we now assume that the radius of the scatterers is small in comparison with the length of the optical wave, such that $ka \ll 1$, then the main contributions come from the dipole components $D_{\pm 1}$ and the set of equations (6) transforms into a set of four equations for four unknowns $D_{\pm 1}$ and $F_{\pm 1}$. The two renormalization factors $G_0$ and $G_2$ enter this set as coefficients.

Introducing the coefficients $2(D, F)_y = (D, F)_1 + (D, F)_{-1}$ and $2\mathrm{i}(D, F)_x = (D, F)_1 - (D, F)_{-1}$, we see that the equations for them split and can easily be solved. We here write only expressions for the dipole moments that determine the diffracted field:

$$D_{x,y} = \begin{pmatrix} \sin\chi \\ -\cos\chi \end{pmatrix}$$

$$\times \frac{J_1'(u)\,J_1(\sqrt{\varepsilon}u) - (1/\sqrt{\varepsilon})\,J_1(u)\,J_1'(\sqrt{\varepsilon}u)}{\big[H_1^1(u) + G_{x,y}J_1(u)\big]\,J_1(\sqrt{\varepsilon}u) - (1/\sqrt{\varepsilon})\big[H_1^1(u) + G_{x,y}J_1(u)\big]\,J_1'(\sqrt{\varepsilon}u)}\,, \tag{7}$$

where $u = ka$ and where the Cartesian renormalization factors are linear combinations of $G_m$,

$$G_x = \sum_{j=1}^{\infty} \left[H_0^1(jkL) - H_2^1(jkL)\right] \cos(kLj \sin\chi)\,,$$

$$G_y = \sum_{j=1}^{\infty} \left[H_0^1(jkL) + H_2^1(jkL)\right] \cos(kLj \sin\chi)\,. \qquad (8)$$

For small $u \ll 1$, the cylinder functions can be expanded into a series, with the result

$$D_{x,y} = \frac{\pi u^2}{4\mathrm{i}} \left\{ \frac{\varepsilon+1}{\varepsilon-1} - \frac{\pi}{4}\,\mathrm{i}u^2(1 + \mathrm{Re}\,G_{x,y}) - \frac{u^2}{8}\left(\left[\varepsilon + 2 - 4\left(\ln\frac{u}{2} + \gamma\right)\right] - 2\pi u^2\,\mathrm{Im}\,G_{x,y}\right)\right\}^{-1}, \qquad (9)$$

which allows a simple physical interpretation. We isolated three groups of terms in the denominator. The first is responsible for the individual quasistatic polarization; the remaining two groups give wave corrections. The imaginary part of the denominator describes the energy losses, including those for emission. The real part gives reactive corrections and determines the resonance frequency. In the case of a real dielectric constant $\varepsilon$, the only channel of losses is radiative losses, which are determined by the second term in the denominator. The collective effects of the renormalization of the fields of emission and 'pressed-to-surface' nonradiative fields are determined by the factors $G_{x,y} = G_0 \mp G_2$, the typical dependences of the real and imaginary parts for which are shown in Fig. 5. Both the real and imaginary parts of the factors $G_{0,2}$ have square-root singularities in the vicinity of the frequencies or incidence angles at which some diffraction maxima become grazing and the field propagating along the $z$ axis is converted into a nonpropagating one, 'pressed' to the lattice of cylinders. It is natural that for finite lattices or for lattices with a disorder, neither an infinite increase nor an infinitely sharp discontinuity occurs. The asymptotic behavior near the diffraction peak, which can be found analytically (for example, see [15], Eqns 8.522), is determined by the real and imaginary parts of the expression

$$G_{0,2} \sim \left[(kL)^2 - (2\pi l \pm kL\sin\chi)^2\right]^{-1/2}, \qquad (10)$$

where $l$ is an integer that corresponds to the order number of the diffraction peak. From the graphs presented in Fig. 5, it can be seen that the behavior of the real and imaginary parts is described by characteristic resonance curves of an asymmetric shape, which is specularly symmetric relative to the singularity point. We note that the factor $G_y$ does not become infinite, apparently because the $y$ components of the dipole moments interact with each other via quasistatic fields, since the dipoles do not emit radiation along themselves.

Now, using the known coefficients (7) and inverting the discrete Fourier transformation, we can find the local multipole coefficients $(D, F)_m^j = (D, F)_m \exp(\mathrm{i}kLj\sin\chi)$ and calculate the scattered field and the fields inside the cylinders. An analysis of the far field with known coefficients is carried out in the standard manner [10], by passing from expansion (3) to an expansion in terms of spatial harmonics of the form

$$B_z^{\text{scatter}} = \sum_l C_l \exp\left[\mathrm{i}\sqrt{k^2 - \left(k\sin\chi + \frac{2\pi l}{L}\right)^2}\,x + \mathrm{i}\left(k\sin\chi + \frac{2\pi l}{L}\right)y\right]. \qquad (11)$$

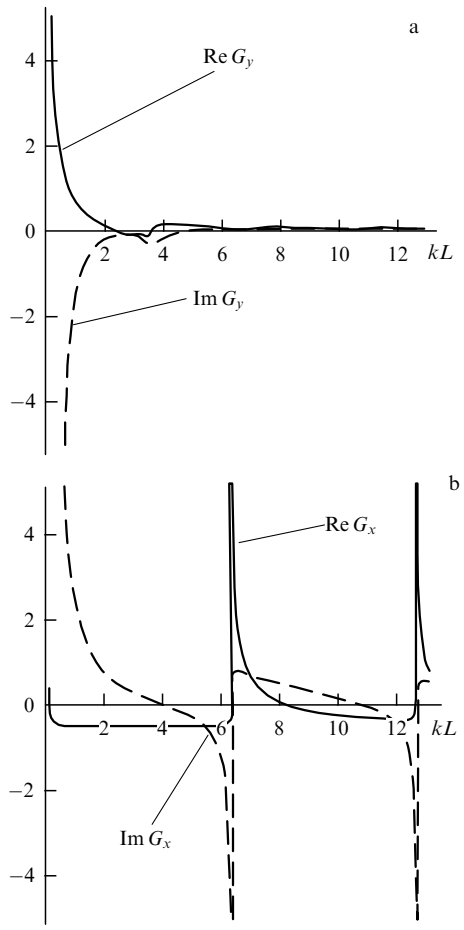


**Figure 5.** Typical frequency dependences of the real (solid curves) and imaginary (dashed curves) parts of the factors of the renormalization of the Cartesian components of the dipole moments (a) $G_y$ and (b) $G_x$, which determine the dissipative and reactive contributions of the collective field. The graphs are plotted at a fixed angle of incidence $\chi$, $\sin\chi = 0.8$.

An analysis of the behavior of the coefficients $C_i$ shows that near the edge of an $l$th diffraction maximum, the power radiated into an appropriate partial wave $P_l \sim \mathrm{Re}\left[k^2 - (k\sin\chi + 2\pi l/L)^2\right]^{1/2} |C_l|^2$ as a function of frequency has a threshold nature. The power radiated into an open channel as a function of frequency has a discontinuity in the derivative. The situation here is in many respects analogous to that characteristic of the behavior of reaction cross sections near reaction thresholds [16].

We now discuss the consequences that can result from the nonperpendicularity of the plane of incidence to the axis of the cylinders and from the presence of gyrotropy caused by the ferromagnetism of the dielectric cylinders. Let the ferromagnet magnetization vector, as previously, be directed along the axes of the cylinders. We first note that the existence of a wave vector of the incident wave parallel to the cylinder axis in the absence of gyrotropy leads to a hybridization of the E and H modes, which until now were accepted to be independent. If we supply the coefficients $D$ and $F$ with an additional index taking values E or H depending on which of the $z$ component is different from zero, and write equations analogous to (6), these equations are no longer be diagonal with respect to this additional index. But the degeneracy in the azimuthal number $m = \pm 1$ is preserved. Then, by introducing Cartesian components, we can reduce the set of the eighth

order for $(D, F)_{\pm 1}^{\mathrm{E,H}}$ to two sets of the fourth order. In this case, as a result of the hybridization of electric and magnetic components, there appear individual resonances determined by the vanishing the factor $\varepsilon + 1$ in the electric components. The renormalization factors $G$, which are responsible for the collective effects, also change; however, because of the retention of the polarization degeneracy, the new $G_y^{\mathrm{E,H}}$ components are then determined by only quasistatic fields, as before.

If we take the gyrotropy into account, then in the dipole approximation, the system analogous to (6) remains a general system of the eighth order, and hybridization must also occur in the vector $x$ and $y$ components of the electric and magnetic dipole moments, causing a mixing of the equations for the $x$ and $y$ projections of the fields and dipole moments. In the dipole components $D_{\pm 1}$, all the resonances are then present, both individual and collective. Because these resonances are shifted in the different components due to the gyrotropy, resonance effects of the polarization plane rotation must be observed in both the reflected and the transmitted radiation. Especially promising for the enhancement of the magnetooptical effects seems to be the diffraction resonance; because of the presence of singularities in frequency in the derivatives of the excitation coefficient of the open channel, the difference in the excitation coefficients of the left-handed and right-handed components are anomalously large, which should lead to anomalously strong Kerr and Faraday effects. It is well possible that a significant enhancement of magnetooptical effects observed recently in experiments [17] is connected precisely with this mechanism.

## 5. Conclusions

We have considered the influence of nanoinhomogeneities on the magnetooptical effects in ferromagnetic films. It has been demonstrated that as a result of the retardation of waves in nanowaveguides and the presence of individual internal resonances in the waveguides and collective effects of multiple scattering, the magnetooptical effects can be considerably enhanced. We expect that the effects of a resonant enhancement of magnetooptical effects can be used for creating new devices for the recording and processing of information and for the diagnostics of magnetic states in composite ferromagnetic films.

**Acknowledgments.** I am very grateful to A A Zharov and A A Andronov for numerous and fruitful discussions. This work was supported in part by the Russian Foundation for Basic Research (project Nos 08-02-00379 and 09-02-00863), Program No. 27 of the Presidium of the Russian Academy of Sciences, and Program No. II.5 of the Division of Physical Sciences, Russian Academy of Sciences.

## References

1. Mishin D D *Magnitnye Materialy* (Magnetic Materials) (Moscow: Vysshaya Shkola, 1991)
2. Genet C, Ebbesen T W *Nature* **445** 39 (2007)
3. Zharov A A, Kurin V V *J. Appl. Phys.* **102** 123514 (2007)
4. White R M *Quantum Theory of Magnetism* 2nd ed. (Berlin: Springer-Verlag, 1983) [Translated into Russian (Moscow: Mir, 1985) p. 197]
5. Mukai R, Uzumaki T, Tanaka A *J. Appl. Phys.* **97** 10N119 (2005)
6. Yuan H et al. *J. Appl. Phys.* **103** 07F513 (2008)
7. Bethe H A *Phys. Rev.* **66** 163 (1944)
8. García de Abajo F J *Rev. Mod. Phys.* **79** 1267 (2007)
9. Chu Y et al. *Appl. Phys. Lett.* **93** 181108 (2008)
10. Meier M, Wokaun A, Liao P F *J. Opt. Soc. Am. B* **2** 931 (1985)
11. Korringa J *Physica* **13** 392 (1947)
12. Kohn W, Rostoker N *Phys. Rev.* **94** 1111 (1954)
13. Wang X et al. *Phys. Rev. B* **47** 4161 (1993)
14. Bever S J, Allebach J P *Appl. Opt.* **31** 3524 (1992)
15. Gradsteyn I S, Ryzhik I M *Tablitsy Integralov, Summ, Ryadov i Proizvedenii* (Table of Integrals, Series, and Products) (Moscow: Fizmatgiz, 1963) [Translated into English (New York: Academic Press, 1965)]
16. Landau L D, Lifshitz E M *Kvantovaya Mekhanika: Nepelyativistskaya Teoriya* (Quantum Mechanics: Non-Relativistic Theory) (Moscow: Nauka, 1989) [Translated into English (Oxford: Pergamon Press, 1977)]
17. Ctistis G et al. *Nano Lett.* **9** 1 (2009)

PACS numbers: 42.25.Gy, **42.55.–f**, **78.67.–n**
DOI: 10.3367/UFNe.0179.200909k.1018

# Superresolution and enhancement in metamaterials

A N Lagarkov, A K Sarychev,
V N Kissel, G Tartakovsky

## 1. Introduction

We discuss the optical and microwave properties of artificial materials that can have negative dielectric and magnetic constants simultaneously. Backward electromagnetic waves can propagate in such metamaterials, which leads to a negative refraction. We discuss some unusual properties of metamaterials, in particular, the effect of superresolution. The large losses predicted in such materials in optics can be compensated by using an amplifying laser medium. We also consider the possibility of designing a nanolaser with a size several dozen times less than the wavelength of light. This article is intended as a general introduction to this thriving field.

More than 100 years have passed since Lamb's work appeared [1], where he first noted the possibility of the existence of backward waves, i.e., unusual wave processes with oppositely directed phase and group velocities. The properties of backward electromagnetic waves were also discussed by Schuster [2]. Almost simultaneously, in the article "Growth of a wave-group when the group velocity is negative," Pocklington [3] showed that in a medium that supports backward waves, a point source excites *convergent* waves, and the group velocity of waves is directed from the source. These works did not attract much attention for almost 40 years, until the well-known work of Mandel'shtam [4] was published, in which he predicted a new physical phenomenon, the negative refraction. This phenomenon can exist only in the case where the refracted waves propagate in a medium that supports backward waves. A discussion of article [4] can be found, for example, in recent work [5].

The next important step was made by Sivukhin in Ref. [6], where it was first shown that in a medium with simultaneously negative dielectric ($\varepsilon$) and magnetic ($\mu$) permeabilities, the group and phase velocities of the wave are oppositely directed. Until the appearance of Ref. [6], this sufficiently fine circumstance remained unnoticed, possibly because the wave equation preserves its form in the case of a simultaneous change of the signs of $\varepsilon$ and $\mu$.

The work by Veselago [7] became a revolutionary step in the study of negative refraction; the idea of a completely original lens was suggested there based on a surprising property of the plane-parallel layer of a material with $\varepsilon = \mu = -1$ (which is now called a metamaterial) to focus the image of an object placed in front of it. Veselago also noted that the optical properties of a metamaterial with negative $\varepsilon$ and $\mu$ can be described by introducing a negative refractive index. Moreover, in the electromagnetic wave propagating in such a metamaterial, the electric field **E**, the magnetic field **H**, and the wave vector $\boldsymbol{\kappa}$ form a *left-handed* triple. In all materials known at that time, these vectors formed a right-handed system. Among other predictions made by Veselago, we mention the change in sign of light pressure in a metamaterial with a negative refractive index. Veselago's work was much ahead of its time. More than 30 years passed after the publication of Ref. [7] until a 'big bang' — the appearance of numerous works on metamaterials — occurred, initiated by Pendri [8], who showed that Veselago's lens has an even more remarkable property: it can create an image of a source without the usual distortions on the wavelength scale. This means that such a lens gives an image whose quality is not confined by the diffraction limit. It is therefore frequently called a superlens. Pendri explained this phenomenon by the amplification in the medium with negative $\varepsilon$ and $\mu$ of waves that exponentially decay in the usual optical materials and media. The first experiment that demonstrated such a superresolution was performed in 2003 [9, 10].

We note that materials with negative $\varepsilon$ and $\mu$ were generally developed and used long before the appearance of Pendri's work. It suffices to recall that the majority of well-conducting metals (gold, silver, aluminum, etc.) have a negative dielectric constant in the visible and infrared spectral ranges. On the other hand, the phenomenon of ferromagnetic resonance, which has been known already for many decades, is very frequently accompanied by the appearance of a negative magnetic permeability. But it is only after the appearance of [8] in 2000 that the creation and study of metamaterials with simultaneously negative $\varepsilon$ and $\mu$ became a new scientific avenue, in which dozens of researchers in many countries worldwide now work.

We pause briefly at the history of metamaterials. In 1952, a monograph was published [11] that contained a chapter devoted to composite materials used for the optimization of the work of radio antennas. To create artificial magnetic permeability, it was proposed to use conducting inclusions in the form of a horseshoe or in the form of a ring resonator with a cut. The equations given in [11] demonstrate the typical resonant behavior of $\mu$ with a negative value at high frequencies. In 1990, monograph [12] was published in Russia, summarizing the results of some studies on the electrodynamics of such composite materials performed at the Institute of Theoretical and Applied Electrodynamics, Russian Academy of Sciences. The results of the further development of this work were published in [13–15]. In [14], experimental studies were described of the dielectric constant of metamaterials containing pieces of metallic microwires (microdipoles) that resonate in the microwave range. Two different values of the length of the microwire pieces were chosen that ensured resonance at two frequencies, and a composite material was demonstrated that had two minima in the frequency dependence of the dielectric constant, both having negative values. The position of the minima is determined by the different length of the conducting inclusions used in the mixture. In [16], it was shown that the inclusions in the form of a pair of conducting cylinders allow obtaining a nonzero magnetic permeability at optical frequencies, which later served as the basis for creating artificial magnetism in the infrared and visible ranges. In 1997 [17], as an outgrowth of this work, experimental data were obtained for a mixture with inclusions in the form of bifilar spirals with negative $\varepsilon$ and $\mu$, and equations were also proposed that satisfactorily reproduced experimental data. These studies were not aimed at obtaining a negative refraction but were part of a systematic work on obtaining metamaterials with an assigned frequency dispersion of the dielectric and magnetic constants. In spite of the large freedom in the selection of shape and concentration of the conducting inclusions, it turned out that the Kramers–Kronig relations impose very stringent constraints on the frequency dependence of the effective parameters. One of the possible applications of these studies is the creation of highly efficient materials for the absorption of radio waves.

## 2. Superresolution in flat focusing systems

The ideas presented in [8] stimulated a detailed study of superresolution mechanisms. In Refs [18–24], which appeared almost simultaneously, it was shown that achieving superresolution requires metamaterials with extremely low losses. In [22, 23], it was noted that the negative influence of Ohmic losses can be substantially reduced in a very thin Veselago lens; therefore, a superresolution can also be achieved under realistic conditions, with the use of accessible metamaterials [9, 10]. In Ref. [23], it was also shown that the focusing and superresolution in a Veselago lens, in contrast to conventional lenses, can be achieved even with a small size of the plate (aperture), which can even be shorter than the wavelength.

In a typical Veselago lens made of a modern metamaterial, the size of the conducting inclusions is comparable to the lens thickness. Therefore, the concept of effective parameters (for example, dielectric and magnetic constants) must be used with care. It has been shown in [16, 25, 26] that for planar metamaterials containing strongly elongated conducting inclusions, the concept of a dielectric constant can be introduced only if the thickness of the material layer exceeds a certain critical value. The distribution of an electromagnetic field in the lens also differs significantly from that obtained in calculations with the use of effective parameters.

Taking the above considerations into account, we selected a flat lens consisting of a single layer of resonators for experiment [10] (Fig. 1). This structure can hardly be considered a plate of a uniform material, not least because it is not possible to clearly define the boundaries of the material in the direction perpendicular to the plate. In a computer model that we developed to describe the operation of the planar superlens, we used the direct solution of the Maxwell equations rather than the effective parameters. In the case under consideration, i.e., for a metamaterial consisting of wire inclusions, solving the Maxwell equations was reduced to solving Pocklington-type equations, which are based on the thin-wire approximation with capacitive load. In particular, the double-coil short spiral used as the inclusion in the metamaterial can be approximated by a metallic ring with a capacitor inserted into the ring break.

In calculations, we also took the finite conductivity of the metal and the corresponding skin effect into account. Our

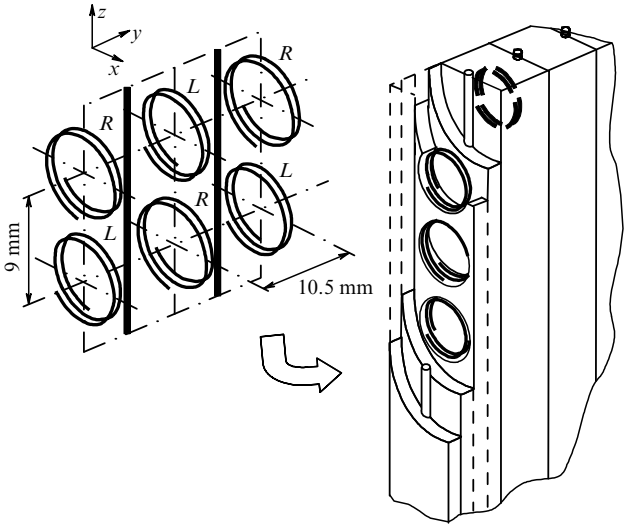


**Figure 1.** Distribution of inclusions in a metamaterial plate.

computational programs allowed calculating the electromagnetic fields generated by different sources both in a finite set of resonators and in an infinite two-dimensional periodic system.

The calculations not only reproduce the effects of focusing and superresolution but also allow comparing the electrodynamic properties of a real metamaterial with those of an ideal completely uniform metasubstance. In particular, it was shown that a plate consisting of only one layer of resonators partly demonstrates the properties of a plate made of an ideal metasubstance. For example, there is a frequency range (positioned somewhat higher than the resonance frequency of inclusions) in which superresolution is observed. This phenomenon can be seen well in Fig. 2a, where the upper part shows a 3D plot of the electric field strength and the lower part shows contour lines calculated both inside and outside the plate. For comparison, Fig. 2b shows the distribution of the field of the same sources in free space. All distances in the figures are given in dimensionless units, i.e., they are multiplied by $k = 2\pi/\lambda$.

On the whole, the plate of our metamaterial can be described as a device that supports backward waves, because a computer simulation indicates the presence of a zone near the plate where the phase and group velocities have opposite directions. However, there is an important difference in the distribution of the local field in a layer of resonators and in an ideal metamaterial. For example, in an ideal uniform metamaterial with $\varepsilon = \mu = -1$, the phase and group velocities of the propagation of electromagnetic waves are opposite to each other only inside the metamaterial layer. The excitation of currents in the layer of resonators forming a real metamaterial leads to the appearance of a spatial zone of backward waves that extends beyond the geometric boundaries of the real metamaterial (the details of the calculation are described in [27, 28]). It is also known [10, 29] that when a plane-parallel layer of an ideal metamaterial is excited, the field energy is concentrated near the farther (relative to the radiation source) face of the layer. This effect is precisely the physical basis of the superresolution phenomenon. In the plate of resonators, an accumulation of energy also occurs, but this energy is concentrated only near specific elements. In what follows, we consider the physical causes for superresolution in a real metamaterial consisting of a planar layer of ringlike resonators and elongated conducting inclusions.

As is known, the electromagnetic field radiated by a point-like source can be represented in the form of a three-dimensional spectrum of plane waves. The coefficients of

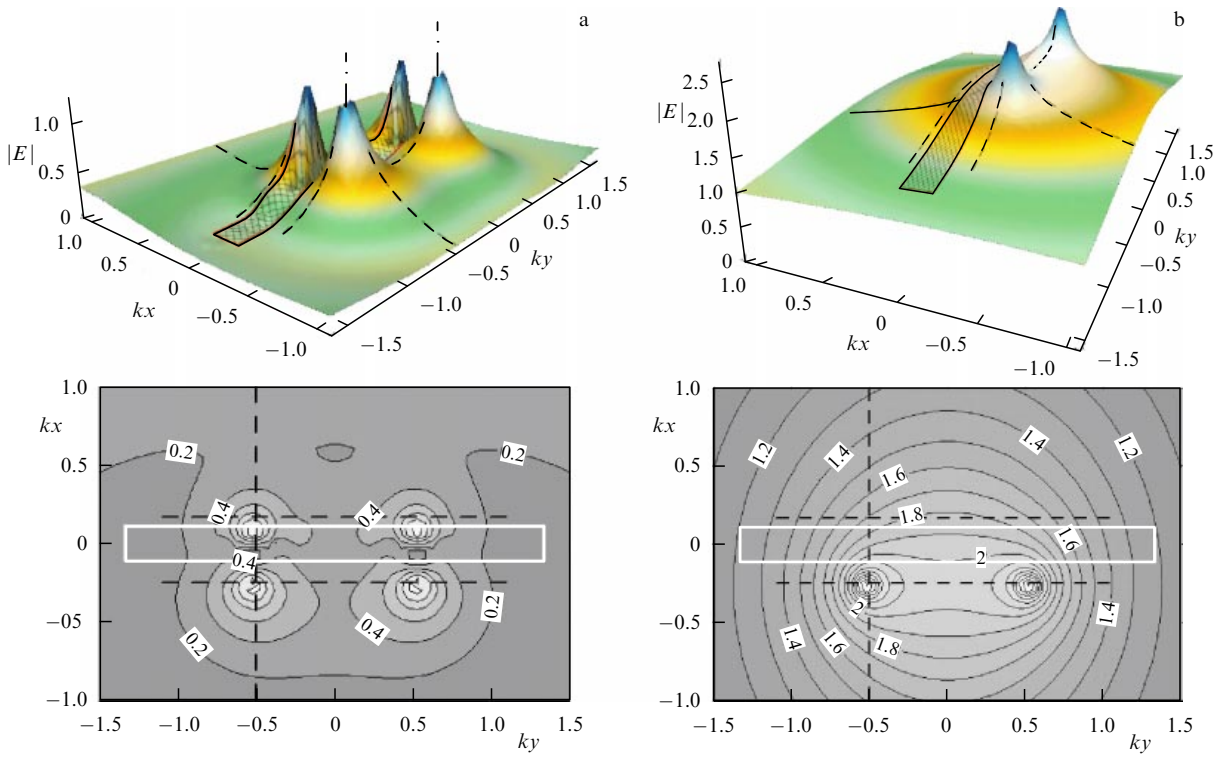


**Figure 2.** Field of linear sources: (a) in the presence of a metamaterial plate and (b) without such a plate.

wave propagation in this case take real and imaginary values. The harmonics with real propagation coefficients are the usual propagating waves. The harmonics with imaginary propagation coefficients describe a wave process that is exponentially damped with distance. To describe propagating waves, a classical beam approach is frequently used. Light beams are focused by a usual optical lens and give an image of an object with a spatial resolution of the order of the light wavelength. For obtaining superresolution, it is necessary to supplement this image with that part of the electromagnetic field that is lost in the damped harmonics.

The problem lies in the fact that exponentially decaying oscillations do not interact with a usual lens so as to be focused into an image, and their amplitude unavoidably decays both in free space and in the usual transparent material. But for obtaining a superresolution, the relation between the amplitudes of the propagating and evanescent waves at the focus must be the same as near the source. According to Pendri's original result, the damped harmonics in the plate of a metamaterial with a negative refractive index begin to increase exponentially when approaching the far (unilluminated) face. In the particular case where $\varepsilon = \mu = -1$, the relation between the amplitudes of the propagating and damped waves is restored at the focus, where an 'exact' image of the object is obtained, which is unrestricted by the diffraction limit. Therefore, we can regard a Veselago lens as an optical device that transmits propagating waves without distortions, but amplifies harmonics with imaginary propagation coefficients, preserving the necessary phase relation.

In Pendri's work and in several dozen subsequent works, objects made of an ideal metasubstance uniquely characterized by their $\varepsilon$ and $\mu$ were examined. We here consider a 'microscopic' theory of superresolution in a metamaterial consisting of electric and magnetic resonators.

For simplicity, we consider a single layer consisting of metallic needles, which play the role of electric resonators, and of split rings, which play the role of magnetic resonators. It is important that the propagating and damped harmonics excite the resonators differently. The difference appears because the electric **E** and magnetic **H** fields are in phase in the propagating waves, and are shifted by 90° in the damped harmonics. The electric and magnetic resonators are excited differently by the propagating and decaying oscillations and, correspondingly, differently emit the secondary electromagnetic field.

Therefore, the electromagnetic response of an electric-resonator–magnetic-resonator pair depends on the nature of the exciting wave, as in the Veselago lens. For example, the current in the resonators (Fig. 3a) determines the magnitudes of the equivalent electric and magnetic moments (Fig. 3b) and, eventually, the magnitudes of the effective $\varepsilon$ and $\mu$. Further studies [27, 28] showed that with the correctly chosen phase and amplitude characteristics of the dipoles (equivalents of the resonators), the system of electric and magnetic dipoles gives clear separate images of point sources in the region behind the plane of a plate made of such a metamaterial; the spacing between the sources is in this case much less than the wavelength. The frequency at which the superresolution effect appears is 3–5% higher than the frequency of the electric and magnetic resonances. If it were possible to introduce effective dielectric and magnetic constants, then this frequency range would correspond to negative values of $\varepsilon$ and $\mu$.

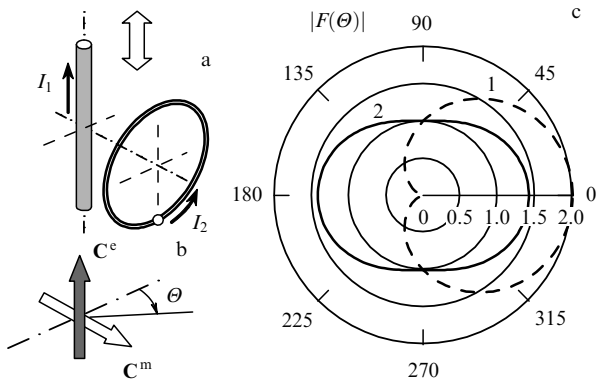


**Figure 3.** (a) Electromagnetic excitation of a pair of interacting resonators (electric and magnetic). (b) Equivalent electric and magnetic dipoles. (c) Directivity diagram for the emission of this pair.

## 3. Magnetic plasmonic resonance in optics. Active metamaterials

In the microwave range, as was shown in Section 2, metamaterials with a negative refractive index are prepared using split ring resonators or spirals, which ensure negative values of the effective magnetic permeability, $\mathrm{Re}\,\mu < 0$. In the microwave range, the metals can be considered almost ideal conductors, because the skin depth ($\sim 1-10$ μm) in them is much less than the characteristic size of metallic inclusions in metamaterials. The magnetic response is reached in the vicinity of the *LC* resonance in spirals or in split rings [17, 30, 31]. Consequently, the frequencies of the *LC* resonances are completely determined by the shape and sizes of inclusions. The resonance appears under specific relations between the size of the split ring and the wavelength of the exciting field. Subsequently, we call the LC resonances in the ideally conducting structures the geometric (G*LC*) resonances.

The situation changes dramatically in the visible and infrared ranges, where the nanosize metallic inclusions behave quite specifically when their thickness becomes less than the skin depth. For example, a plasmonic resonance appears as a result of collective oscillations of electrons. Because of these oscillations, the dielectric constant of metals $\varepsilon_{\mathrm{m}}$ is negative in the visible and infrared ranges. The plasmonic resonances cause many interesting optical phenomena, e.g., the propagation of surface plasmons, anomalous absorption, giant Raman scattering, and light supertransmission (see, e.g., [31, 32]).

The near-field superresolution also appears as a result of the excitation of plasmons in metamaterials with $\varepsilon = -1$ [6]. The near-field superresolution can be explained on the basis of the elementary solution of a problem in electrostatics (see, e.g., book of problems [41], problem no. 209). The plasmonic response of metals is the basic reason why the G*LC* resonance method is not directly applicable in optics.

Optical metamaterials with a negative refractive index were first demonstrated in [34–36]. In [34, 35], a plasmonic resonance that appears in a system of parallel nanowires was used. Such resonances were first examined in our previous works [16, 31, 37]. In [36], a negative real part of the refractive index was observed at the wavelength 2.0 μm in a system consisting of two parallel gold nanofilms with the openings of a size much smaller than the wavelength. The metallic

connections between the openings play the role of nanoantennas analogous to pairs of nanowires.

The first work on obtaining and studying optical metamaterials was continued by other successful experiments [38–43]. For example, the creation of a prism from an optical metamaterial and the demonstration of a negative deviation of a light beam were described in [43]. The negative optical magnetic permeability was first announced in [44]. But we believe that the geometry used in that experiment (vertical metallic columns perpendicular to the film plane) does not allow exciting magnetic resonances in the case of normal incidence of light on the film. Indeed, irrespective of the polarization of the incident wave, the electric field is perpendicular to the axis of the metallic columns and cannot excite closed electric currents that flow in opposite directions along the metal inclusions. Some other problems related to the experiment in [44] were discussed in [45].

As was noted above, the losses are most important in the microwave range. With decreasing the wavelength (shifting it toward the visible range), the Ohmic losses become the decisive factor limiting the application of metamaterials [46, 47]. In particular, these losses radically decrease the chances of obtaining superresolution and make the creation of a flat optical Veselago lens with a superresolution virtually impossible. In other optical instruments based on the use of metamaterials, such as a hyperlens [48–52] or an invisibility device (a 'cloak') [53–56], the losses do not lead to the disappearance of efficiency, but sharply reduce the optical power of promising instruments. The problem of losses can be solved by using amplifying laser materials.

A plasmonic resonance in a metallic nanoantenna placed in an amplifying medium can be used for the excitation of magnetic and electric dipoles. The amplifying medium increases the amplitude of the excited dipoles and can in principle lead to the complete compensation of losses in the metamaterial. Because the enhancement of the electromagnetic field in a laser material implies the presence of an external energy source, this means that a metamaterial including an active medium is a dissipative system. Consequently, the substantial limitations imposed by the Kronig–Kramers relations on the behavior of the effective parameters become unobvious.

As an example of the use of an amplifying medium, we consider the phenomenon of the magnetic plasmonic resonance (MPR) in an optical nanoantenna placed into such a medium [69]. An MPR has a very important property: its frequency depends on the structure of the nanoantenna but not on its overall size. An MPR can be excited in a metallic 'nanohorseshoe' (Fig. 4). Structures of this form act as optical antennas, concentrating electric and magnetic fields on a scale that is much smaller than the wavelength of light. The magnetic response of nanohorseshoes is characterized by the magnetic polarizability $\alpha_M$, which exhibits a Lorentz resonance: the real part reverses sign near the resonance frequency and becomes negative, as is necessary for creating optical metamaterials with a negative magnetic permeability.

The concept of a magnetic plasmonic resonance, which leads to optical magnetism, is relatively new and, of course, contradicts the known concept [57] of the impossibility of magnetism in optics. However, this only seem to be a contradiction: the authors of [57] mean the microscopic magnetism, while the negative magnetism we discuss here arises at a mesoscopic level, as a result of collective electron motion.

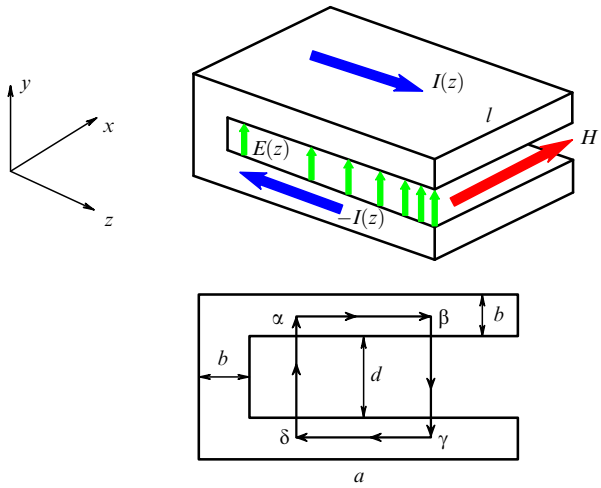


**Figure 4.** Nanoantenna in the form of a horseshoe (nanohorseshoe). The parameters used in computer simulation: $a = 300$ nm, $d = 70$ nm, and $b = 34$ nm.

Our discussion in what follows is based on the consideration of the collective effects in a metallic nanohorseshoe. The results obtained can easily be extended to other antennas.

We consider the interaction of a nanohorseshoe with an amplifying medium simulated by a two-level amplifying system (TLS) represented, for example, by quantum dots or molecules of a dye. The metallic horseshoe that interacts with the TLS is arguably the simplest plasmon system; based on this system, we can study the basic properties of active metamaterials, including processes of nanolasing. The nonradiative energy transfer from the active medium to quasistatic plasmonic oscillations has been discussed in [58]. The processes of propagation of a surface plasmon–polariton at the boundary between a metal and an active medium have been studied since the 1960s [59–63]. The superresolution in the near-field lens due to the compensation of losses in the presence of an amplifying medium was discussed in [64]. Work on active metamaterials performed before 2006 was discussed in review [41]. The first experimental and theoretical work on plasmonic resonance in metallic nanoparticles placed into an active medium was performed in [65–67]. The work that is nearest to our approach is [68], where a dipole laser was considered.

We have already mentioned that the simple compensation of losses in metamaterials does not necessarily lead directly to an increase in superresolution. Nevertheless, active metamaterials offer new possibilities for the optimization of the operation of superresolution optical systems. The active metamaterials are also important for practical applications different from those related to superresolution. For example, the plasmonic nanolaser discussed in Section 4 is a source of coherent emission, whose size can be several dozen times less than the wavelength of light. Such a nanolaser can be regarded as a nanogenerator for the power supply of future plasmonic devices, e.g., those intended for information processing.

We consider a metallic nanohorseshoe with a TLS introduced into it. The population inversion in the TLS is ensured by external pumping. The pumping can be optical or electrical, when the carriers are injected into the TLS, for example, into a quantum dot, from the surrounding material. The TLS interacts with the electromagnetic field that is

excited inside the nanohorseshoe. In the equations of motion, we use a phenomenological description of pumping, characterizing the TLS by the value of the stationary inversion of the population. In other words, we characterize the TLS by the level of inversion that would exist if the TLS did not interact with the nanohorseshoe. An external AC magnetic field $\mathbf{H} = (H_0(t), 0, 0)$ is applied in the plane of the nanohorseshoe, as is shown in Fig. 4. The displacement currents in the gap of the horseshoe close the circuit.

The closed electric current $I(z)$ flowing in the nanohorseshoe generates the magnetic field $H(z) = 4\pi I(z)/c$ in the gap, where $I(z)$ is the density of the surface current in the upper plate of the capacitor (i.e., in the plate $\alpha\beta$ in Fig. 4) and $c$ is the speed of light. To obtain a closed equation for the current, we integrate the Maxwell equation $\operatorname{rot}\mathbf{E} = -\dot{\mathbf{H}}/c$, which expresses the Faraday induction law, along the contour $\alpha\beta\gamma\delta$ and obtain the equation

$$\left[2I(z)\,Z - \frac{\partial U}{\partial z}\right]\Delta z = -\frac{d}{c}\left(\frac{4\pi}{c}\,\dot{I}(z) + \dot{H}_0\right)\Delta z\,, \tag{1}$$

where $\Delta z$ is the distance between the points $\alpha$ and $\beta$ along the integration contour shown in Fig. 4, dots denote time derivatives, $Z = 1/(\sigma b) = 4\mathrm{i}\pi/(\varepsilon_{\mathrm{m}}\omega b)$ is the surface impedance, and $\varepsilon_{\mathrm{m}}$ is the complex dielectric constant of the metal.

We substitute the potential difference $U(z) = E_y(z)\,d = -4\pi(Q(z) + P(z))\,d$ in (1), where $Q(z)$ is the charge per unit area and $P(z)$ is the polarization of the medium inside the nanohorseshoe. We then differentiate both parts of Eqn (1) with respect to time and use the charge conservation law $\partial I/\partial z = -\partial I_1/\partial z = -\partial Q/\partial t$, where $I_1$ is the current in the lower plate. Thus, we obtain the basic equation for the current in the nanoantenna:

$$\frac{\partial^2 I(z,t)}{\partial z^2} - \frac{\partial \dot{P}(z,t)}{\partial z} - \frac{Z}{2\pi d}\,\dot{I}(z,t) = \frac{1}{4\pi c}\left[\frac{4\pi}{c}\,\ddot{I}(z) + \ddot{H}_0\right]. \tag{2}$$

This equation is analogous to the well-known telegrapher equation [57, p. 91]. For determining the polarization $P$, a matter equation must be added to Eqn (2). The polarization of the medium inside the nanohorseshoe is the sum of two polarizations: $P = P_1 + P_2$, where $P_1 = \chi_1 E_y$ is the usual polarization of a dielectric and $P_2$ is the 'anomalous' polarization due to pumping of the active medium; $\chi_1$ denotes the usual (nonresonant) polarizability of the medium. We substitute $P = \chi_1 E_y + P_2$ in (1) and obtain

$$\frac{\partial^2 I(z,t)}{\partial z^2} - \frac{\partial \dot{P}_2(z,t)}{\partial z} - \frac{Z\varepsilon_{\mathrm{d}}}{2\pi d}\,\dot{I}(z,t) = \frac{\varepsilon_{\mathrm{d}}}{4\pi c}\left[\frac{4\pi}{c}\,\ddot{I}(z) + \ddot{H}_0\right], \tag{3}$$

where the polarizability $\chi_1$ now enters the 'regular' part of the dielectric constant $\varepsilon_{\mathrm{d}} = 1 + 4\pi\chi_1$.

We first consider the simplest case where the laser polarizability $P_2$ is linear in the applied field, $P_2 = \chi_2 E_y$. This is possible if we are far from the generation threshold and therefore the interaction with the plasmons does not lead to the depletion of the upper level of the TLS. We also assume that the external field oscillates with a frequency $\omega$, $H_0(t) = H_0\exp(-\mathrm{i}\omega t)$. Under these assumptions, Eqn (3) takes the form

$$\frac{\partial^2 I(z)}{\partial z^2} = -g^2 I(z) - \frac{\varepsilon_{\mathrm{d}}\omega k}{4\pi}\,H_0\,, \tag{4}$$

where the coordinate $z$ varies in the range $0 < z < a$, and the coordinates $z = 0$ and $z = a$ correspond to the beginning and end of the nanohorseshoe, such that $\mathrm{d}I(0)/\mathrm{d}z = I(a) = 0$; $k = \omega/c$; and the wave vector of the plasmon $g$ is determined from the equation

$$g^2 = \varepsilon_{\mathrm{d}}\,k^2 - \frac{2\varepsilon_{\mathrm{d}}}{bd\varepsilon_{\mathrm{m}}}\,, \tag{5}$$

where the dielectric constant includes both the ordinary part and the contribution of the TLS. The second term in the right-hand side of Eqn (5) can be represented in the form $\sim k^2(\delta/b)^2$, where $b$ is the characteristic size of the system (for example, the thickness of the capacitor plate), and $\delta$ is the skin depth. If $\delta \ll b$, which is typical of the microwave range, we obtain the usual G$LC$-antenna resonance. In the opposite case $k^2 bd|\varepsilon_{\mathrm{m}}| \ll 1$, the parameter $g = \sqrt{-2\varepsilon_{\mathrm{d}}/(\varepsilon_{\mathrm{m}} bd)}$ is independent of the absolute length of the nanohorseshoe and does not depend explicitly on the frequency. This is a situation characteristic of the MPR, which occurs for the nanohorseshoes in the visible range [69]. It is interesting that the electric field is nonpotential under the conditions of MPR; the $E_y$ component depends on the coordinate $z$, while the component of the electric field $E_z$ depends on the coordinate $y$. The presence of a solenoidal optical field at scales much smaller than the wavelength of light is a characteristic feature of the MPR.

The electric current $I(x)$ found from Eqn (4) allows calculating the magnetic moment of the nanohorseshoe. The magnetic moment $m$ has a resonance if the condition $ga = \pi/2$ is satisfied as the magnitude of $m$ becomes large. We note that the resonance condition is satisfied not for the absolute size of the nanohorseshoe but for the ratio of its length to its width. For a typical metal, the frequency behavior of the dielectric constant is qualitatively described by the Drude formula $\varepsilon_{\mathrm{m}} = -(\omega_{\mathrm{p}}/\omega)^2(1 + \omega_\tau/\omega)^{-1}$, where $\omega_{\mathrm{p}}$ is the plasmonic frequency and $\omega_\tau$ is the relaxation frequency, which are estimated, for example, as $\hbar\omega_{\mathrm{p}} = 9.6$ eV and $\hbar\omega_\tau = 0.02$ eV for silver. In this notation, the magnetic moment of the horseshoe is written as

$$\alpha_{\mathrm{M}} = V\,\frac{bd\omega_{\mathrm{p}}^2}{\pi\lambda^2\omega_{\mathrm{r}}^2}\,\frac{1}{1 - \omega/\omega_{\mathrm{r}} - \mathrm{i}(\varkappa_{\mathrm{m}} + \varkappa_{\mathrm{d}})/2}\,, \tag{6}$$

where the resonance frequency is $\omega_{\mathrm{r}} = \omega_{\mathrm{p}}\pi\sqrt{bd/[8\operatorname{Re}(\varepsilon_{\mathrm{d}})a^2]}$, $V$ is the volume of the horseshoe, $\varkappa_{\mathrm{m}}$ is the dimensionless loss in the metal ($\varkappa_{\mathrm{m}} = \operatorname{Im}\varepsilon_{\mathrm{m}}/\operatorname{Re}\varepsilon_{\mathrm{m}} \approx \omega_\tau/\omega \ll 1$), and $\varkappa_{\mathrm{d}}$ is the dimensionless loss in the dielectric, also assumed to be small: $\varkappa_{\mathrm{d}} = \operatorname{Im}\varepsilon_{\mathrm{d}}/\operatorname{Re}\varepsilon_{\mathrm{d}} \ll 1$.

Expression (6) for $\alpha_{\mathrm{M}}$ contains the factor $bd/\lambda^2 \ll 1$, which is small for the nanohorseshoes; however, near the resonance, the condition $|\alpha_{\mathrm{M}}| \gg 1$ can be satisfied in the visible and infrared ranges as a result of the high quality of the MPR. The presence of a frequency range where the magnetic polarizability $\alpha_{\mathrm{M}}$ is negative and large in magnitude allows creating optical metamaterials with a negative magnetic permeability.

The distribution of the magnetic field in the nanohorseshoe for a frequency close to the resonance is shown in Fig. 5. The behavior of the optical magnetic permeability for a metamaterial consisting of nanohorseshoes is shown in Fig. 6. If the dielectric is an active medium, then the dimensionless losses $\varkappa_{\mathrm{d}}$ become negative under pumping. This leads to a compensation of losses in the metal. As the

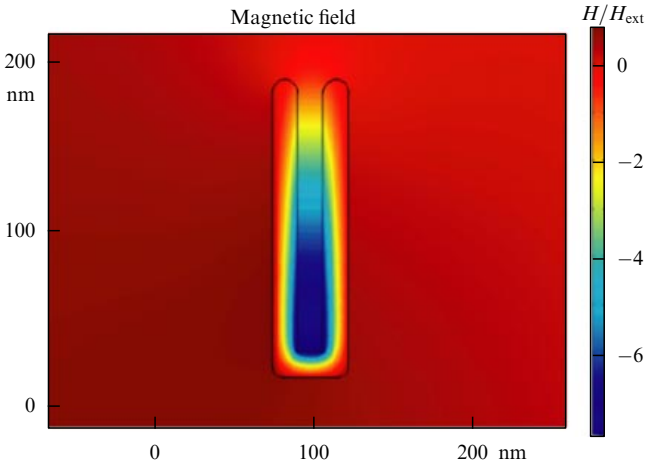


**Figure 5.** Magnetic plasmonic resonance in a silver nanohoof excited by an external magnetic field $H_{ext}$ perpendicular to the figure plane. The external field wavelength is $\lambda = 1.5$ μm; $\varepsilon_d = 2$. The magnetic field $H$ inside the hoof is directed against the external field, which corresponds to a negative polarizability.

losses are compensated due to the active medium and the total losses $\varkappa = \varkappa_m + \varkappa_d$ decrease, the absorption line (dashed curve in Fig. 6) becomes narrower. At some moment, the losses become negative, which indicates the loss of stability. The metamaterial begins lasing.

## 4. Interaction of plasmons with an amplifying medium. Plasmonic nanolaser

To explain the nature of plasmonic lasing, we consider the microscopic model suggested in [70–72]. In this model, the equations of motion are derived from quantum mechanics, but they are solved without taking the fluctuations into account and with quantum mechanical operators regarded as complex quantities. This approximation allows obtaining an analytic solution and carrying out a qualitative analysis of the system shown in Figs 4 and 7.

The Hamiltonian of a nanoantenna interacting with a TLS is given by the sum of Hamiltonians $H = H_0 + H_{TLS} + V_{int} + \Gamma$, where $H_0$ and $H_{TLS}$ respectively describe the nanohorseshoes and the TLSs, $V_{int} = -P_2\langle E_y\rangle Sd = -p\langle E_y\rangle NSd$ is the operator of the averaged interaction between a TLS and a nanohorseshoe, $p$ is the dipole moment operator, $N$ is the density of TLSs in the nanohorseshoe, $S$ is the area of the nanohorseshoe, $d$ is the distance between the plates of the capacitor, and $\Gamma$ describes the effects of dissipation and pumping.

The electrons and the related electric field oscillate with a frequency $\omega$ close to the MPR frequency. These oscillations are plasmons in the nanoantenna. We regard the electric charge and field as classical quantities.

We introduce operators $b$ and $b^+$ corresponding to the transition between the excited and ground states of the TLS. Then the Hamiltonian of the TLS takes the form $H_{TLS} = \hbar\omega_2 b^+ b$. The operator of the dipole moment can be

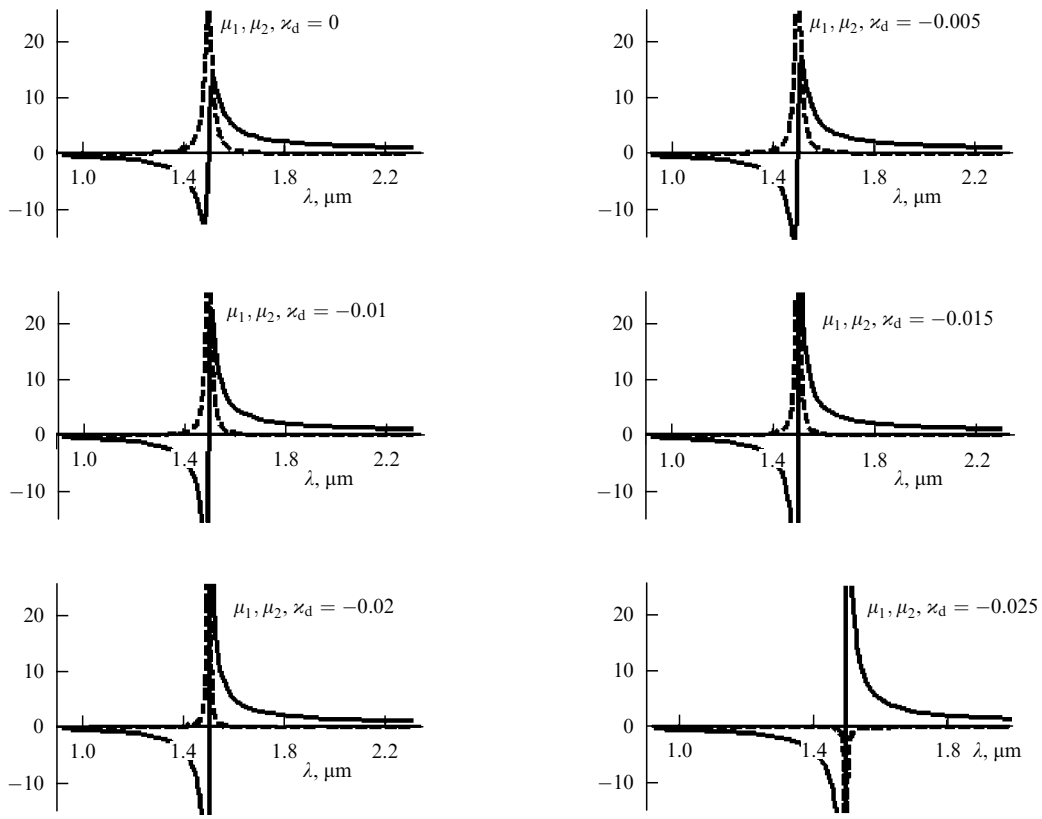


**Figure 6.** Effective magnetic permeability $\mu = \mu_1 + i\mu_2$ of a metamaterial made of silver nanohorseshoes placed in an active medium with the dielectric constant $\varepsilon_d = 4(1 + i\varkappa_d)$, where the loss factor is negative ($\varkappa < 0$) because of the pumping of the medium. The nanohorseshoe parameters used in computer simulation are $a = 300$ nm, $d = 70$ nm, and $b = 34$ nm; the bulk concentration of the nanohorseshoes is $p = 0.3$. The real part of the magnetic permeability $\mu_1$ is shown by the solid line, and the imaginary part $\mu_2$ is shown by the dashed line. Upon passing through the value $\varkappa_d = -0.025$, the metamaterial loses stability and starts lasing.

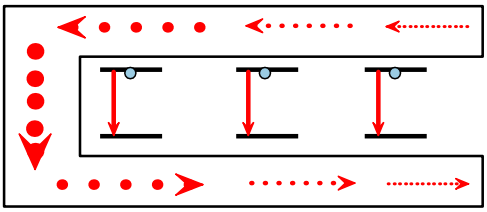

**Figure 7.** At plasmon oscillating in a nanohorseshoe (dotted lines); its amplitude increases due to the interaction with excited two-level systems, which give their energy to the plasmon.

written as

$$P_2 = \Pi b \exp(-\mathrm{i}\omega t) + \Pi^* b^+ \exp(\mathrm{i}\omega t)\,, \tag{7}$$

where $\Pi \approx \langle g|\, r\, |e\rangle$ is the matrix element of the TLS dipole operator. We also introduce the population inversion operator $D(t) = n_\mathrm{g}(t) - n_\mathrm{e}(t)$, where $n_\mathrm{e}(t) = b^+ b$ and $n_\mathrm{g}(t) = bb^+$ are the respective operators of the population of the upper and lower levels. We assume that the TLS oscillates between the excited and ground levels with a frequency $\omega$ that is close to the frequency $\omega_2$ ($\hbar\omega_2$ is the difference between the energy levels of the TLS).

Using known commutation relations between the operators $b$, $b^+$, and $n_{\mathrm{e,g}}$, we can derive the Heisenberg equation of motion for operators $\mathrm{i}\hbar\dot{b} = [b, H]$ and $\mathrm{i}\hbar\dot{D} = [D, H]$. We consider lasing as the process of oscillations of the electric charge in the nanohoof even in the absence of an external magnetic field. We assume that this is a stationary process, i.e., the oscillation amplitude does not vary with time. Then the equation for the charge and the equation for $b$ and $D$ can be written as

$$(\mathrm{i}\delta + \gamma)\, q_2 - \mathrm{i}b = 0\,, \quad (\mathrm{i}\Delta + \Gamma)\, b - \mathrm{i}AD q_2 = 0\,, \tag{8}$$

$$\frac{D - D_0}{\tau} - 2\mathrm{i}A(q_2^* b - q_2 b^+) = 0\,,$$

where $q_2 = q/(SN\Pi)$ is the dimensionless electric charge, $\delta = 1 - (\omega/\omega_\mathrm{r})^2$, $\gamma = (\varepsilon''_\mathrm{m}/|\varepsilon'_\mathrm{m}|)(\omega/\omega_\mathrm{r})^2 \approx \varepsilon''_\mathrm{m}/|\varepsilon'_\mathrm{m}|$, $\Delta = (\omega_2 - \omega)/\omega_\mathrm{r}$ [70–72], and the terms with $\Gamma$ and $\tau$ respectively take the processes of relaxation of the dipole moment and population into account. In the 'laser' terminology, these are the processes of transverse and longitudinal relaxation; $D_0$ is the value of the population that would be achieved by pumping if the TLS did not interact with the nanohorseshoe. We assume that we are dealing with inversion, i.e., $D_0 < 0$. Disregarding quantum fluctuations and correlations, $D$ and $b$ can be considered complex quantities with the replacement $b^+ \to b^*$. The dimensionless constant is written as

$$A = \frac{4\pi N|\Pi|^2}{\omega_\mathrm{r}\hbar n^2} > 0\,,$$

where $N$ is the bulk density of TLSs and $n$ is the refractive index of the medium in which the TLSs are located, for example, quantum dots. Equation (8) has a nontrivial solution only if the following conditions, which are simultaneously the conditions of lasing, are satisfied:

$$\frac{\Delta}{\Gamma} = -\frac{\delta}{\gamma}\,, \quad \left(\frac{\delta}{\gamma}\right)^2 + 1 + \frac{AD_0}{\Gamma\gamma} = 0\,. \tag{9}$$

The first condition gives the frequency of lasing, which always lies between the MPR frequency $\omega_\mathrm{r}$ and the TLS resonance frequency $\omega_2$. All terms in (9) are positive, except the population in the second lasing condition. Consequently, this condition is satisfied only in the case of inversion $n_\mathrm{e} > n_\mathrm{g}$, when $D_0 < 0$. According to the definition, $D_0$ cannot be less than $-1$, which corresponds to the case where all the TLSs are in an excited state. Thus, we obtain the condition necessary for lasing: $A/(\Gamma\gamma) > 1$. As soon as the second condition in (9) is satisfied, the interaction between the TLS and the nanohorseshoe leads to coherent oscillations of the electric charge, current, and magnetic moment even in the absence of an external electromagnetic field.

The lasing condition can be expressed in terms of the amplification coefficient $G$ in the active medium located in the nanohorseshoe. The amplification in the medium must be large, and hence the inequality

$$\frac{G\lambda}{2\pi n\gamma} > 1 \tag{10}$$

is satisfied, where $\gamma = \varepsilon'_\mathrm{m}/|\varepsilon''_\mathrm{m}| \ll 1$ is the dimensionless factor of losses in the metal and $n \sim 1$ is the refractive index.

We note that the lasing condition depends on the amplification in the active medium and on the losses in the metal. We assume that this is a universal condition for the operation of a plasmonic nanolaser with any configuration of the metallic nanoantenna. For example, a silver nanoantenna lases at the wavelength 1.5 μm if the active medium that fills it has an amplification factor larger than $G_\mathrm{c} \approx 5 \times 10^3$ cm$^{-1}$ at this frequency.

We now consider the effect of an external magnetic field on the operation of a nanolaser. A high-frequency magnetic field excites currents in the nanohorseshoe and acts as a driving force. In the absence of this force, the plasmonic nanolaser, which should be regarded as a nonlinear oscillator, self-oscillates and moves along its limit cycle with the lasing frequency given by Eqn (9). When we apply an external force, the plasmonic laser continues moving along the same limit cycle but already with the frequency of the external force. In other words, an external electromagnetic wave can retune the nanolaser. This fantastic possibility requires further study.

## 5. Conclusions

We see that metamaterials offer new possibilities for developing different devices in the microwave and visible ranges, such as focusing systems, nanolasers, absorbers, resonators, and many other devices. The development of new electromagnetic materials, which starts from the construction of unit cells with predetermined properties that may or may not exist in nature, is a new technique that opens unique prospects. The spectrum of the potential applications of metamaterials that is discussed in the contemporary literature extends from unique sensors of Raman scattering to the creation of cloaking devices ('magic caps' and 'magic carpets'). Moreover, work on the creation and analysis of mechanical (e.g., acoustic) metamaterials has actively been developed recently. Nevertheless, we emphasize that in spite of all the progress achieved in experimental and theoretical studies, no commercially successful metamaterials or devices based on them have been developed so far. This is partly connected with the problem of losses, which was discussed in Sections 2 and 3. We attempted to show that the physics of metamaterials is

very interesting not only because of its attractive potential applications but also in and of itself, and that many fundamental problems remain unsolved to date.

**Acknowledgments.** This work was supported in part by the Russian Foundation for Basic Research, project No. 09-02-01519.

## References


1. Lamb H *Proc. London Math. Soc. Ser. 2* **1** 473 (1904)
2. Schuster A, Sir *An Introduction to the Theory of Optics* (London: E. Arnold, 1904) p. 313
3. Pocklington H C *Nature* **71** 607 (1905)
4. Mandel'shtam L I *Lektsii po Optike, Teorii Otnositel'nosti i Kvantovoi Mekhanike* (Lectures on Optics, Theory of Relativity, and Quantum Mechanics) (Moscow: Nauka, 1972) p. 431 (the lecture was presented on May 5, 1944)
5. Agranovich V M, Gartstein Yu N *Usp. Fiz. Nauk* **176** 1051 (2006) [*Phys. Usp.* **49** 1029 (2006)]
6. Sivukhin D V *Opt. Spektrosk.* **3** 308 (1957)
7. Veselago V G *Usp. Fiz. Nauk* **92** 517 (1967) [*Sov. Phys. Usp.* **10** 509 (1968)]
8. Pendry J B *Phys. Rev. Lett.* **85** 3966 (2000)
9. Lagarkov A N, Kissel V N, in *Proc. of the 2nd Intern. Conf. on Materials for Advanced Technologies, Sym. F: Electromagnetic Materials, SUNTEC, Singapore, 7–12 December 2003* (Eds Lim Hock et al.) (Singapore: World Scientific, 2003) p. 157
10. Lagarkov A N, Kissel V N *Phys. Rev. Lett.* **92** 077401 (2004)
11. Schelkunoff S A, Friis H T *Antennas: Theory and Practice* (New York: Wiley, 1952)
12. Antonov A S et al. *Elektricheskie i Magnitnye Svoistva Perkolyatsionnykh Sistem* (Electrical and Magnetic Properties of Percolation Systems) (Ed. A N Lagar'kov) (Moscow: IVTAN, 1990)
13. Lagarkov A N, Panina L V, Sarychev A K, Smychkovich Y R, presented at the 1990 MRS Spring Meeting Symp., April 16–21, 1990, San Francisco, Calif., S 9.3 (1990)
14. Kolesnikov A N et al., in *Optical and Electrical Properties of Polymers* No. 214 (Eds J A Emerson, J M Torkelson) (Pittsburgh: Material Research Society, 1991) p. 119
15. Lagarkov A N et al. *J. Electromagn. Waves Appl.* **6** 1159 (1992)
16. Lagarkov A N, Sarychev A K *Phys. Rev. B* **53** 6318 (1996)
17. Lagarkov A N et al. *Electromagnetics* **17** 213 (1997)
18. Fang N, Zhang X *Appl. Phys. Lett.* **82** 161 (2003)
19. Smith D R et al. *Appl. Phys. Lett.* **82** 1506 (2003)
20. Ong C K, Rao X S, in *Proc. of the 2nd Intern. Conf. on Materials for Advanced Technologies, Sym. F: Electromagnetic Materials, SUNTEC, Singapore, 7–12 December 2003* (Eds Lim Hock et al.) (Singapore: World Scientific, 2003) p. 123
21. Rao X S, Ong C K *Phys. Rev. E* **68** 067601 (2003)
22. Kissel V N, Lagarkov A N *Proc. of the 2nd Intern. Conf. on Materials for Advanced Technologies, Sym. F: Electromagnetic Materials, SUNTEC, Singapore, 7–12 December 2003* (Eds Lim Hock et al.) (Singapore: World Scientific, 2003) p. 145
23. Lagarkov A N, Kisel' V N *Dokl. Ross. Akad. Nauk* **394** 40 (2004) [*Dokl. Phys.* **49** 5 (2004)]
24. Podolskiy V A, Narimanov E E *Opt. Lett.* **30** 75 (2005)
25. Vinogradov A P, Makhnovskii D P, Rozanov K N *Radiotekh. Elektron.* **44** 341 (1999) [*J. Commun. Technol. Electron.* **44** 317 (1999)]
26. Liu L et al. *Electromagnetics* **25** 69 (2005)
27. Kissel V N, Lagar'kov A N *Phys. Rev. B* **72** 085111 (2005)
28. Lagarkov A N, Kisel V N *Physica B* **394** 163 (2007)
29. Cui T J et al. *Phys. Lett. A* **323** 484 (2004)
30. Pendry J B et al. *IEEE Trans. Microwave Theory Tech.* **47** 2075 (1999)
31. Sarychev A K, Shalaev V M *Electrodynamics of Metamaterials* (Singapore: World Scientific, 2007)
32. Sarychev A K, Shalaev V M *Phys. Rep.* **335** 275 (2000)
33. Batygin V V, Toptygin I N *Sbornik Zadach po Elektrodinamike* (Problems in Electrodynamics) (Moscow: Nauka, 1970) [Translated into English (London: Academic Press, 1978)]
34. Shalaev V M et al. *Opt. Lett.* **30** 3356 (2005)
35. Drachev V P et al. *Laser Phys. Lett.* **3** 49 (2006)
36. Zhang S et al. *Phys. Rev. Lett.* **95** 137404 (2005)
37. Sarychev A K, Shalaev V M *Proc. SPIE* **5508** 128 (2004)
38. Dolling G et al. *Opt. Lett.* **31** 1800 (2006)
39. Dolling G et al. *Science* **312** 892 (2006)
40. Dolling G et al. *Opt. Lett.* **32** 53 (2007)
41. Klar T A et al. *IEEE J. Select. Topics Quantum Electron.* **12** 1106 (2006)
42. Shalaev V M *Nature Photon.* **1** 41 (2007)
43. Valentine J et al. *Nature* **455** 376 (2008)
44. Grigorenko A N et al. *Nature* **438** 335 (2005)
45. Kildishev A V et al. *Opt. Lett.* **32** 1510 (2007)
46. Dimmock J *Opt. Express* **11** 2397 (2003)
47. Zhou J et al. *Phys. Rev. Lett.* **95** 223902 (2005)
48. Jacob Z, Alekseyev L V, Narimanov E *Opt. Express* **14** 8247 (2006)
49. Salandrino A, Engheta N *Phys. Rev. B* **74** 075103 (2006)
50. Govyadinov A A, Podolskiy V A *Phys. Rev. B* **73** 155108 (2006)
51. Liu Z et al. *Science* **315** 1686 (2007)
52. Smolyaninov I I, Hung Y-J, Davis C C *Science* **315** 1699 (2007)
53. Pendry J B, Schurig D, Smith D R *Science* **312** 1780 (2006)
54. Leonhardt U *Science* **312** 1777 (2006)
55. Li J, Pendry J B *Phys. Rev. Lett.* **101** 203901 (2008)
56. Ma Y G et al. *Nature Mater.* **8** 639 (2009)
57. Landau L D, Lifshitz E M, Pitaevskii L P *Elektrodinamika Sploshnykh Sred* (Electrodynamics of Continuous Media) (Moscow: Fizmatlit, 2001) [Translated into English (Oxford: Pergamon Press, 1984)]
58. Bergman D J, Stockman M I *Phys. Rev. Lett.* **90** 027402 (2003)
59. Kogan B, Volkov V, Lebedev S *Pis'ma Zh. Eksp. Teor. Fiz.* **16** 144 (1972) [*JETP Lett.* **16** 100 (1972)]
60. Plotz G, Simon H J, Tucciarone J M *J. Opt. Soc. Am.* **69** 419 (1979)
61. Sudarkin A, Demkovich P *Zh. Tekh. Fiz.* **59** (7) 86 (1989) [*Sov. Phys. Tech. Phys.* **34** 764 (1989)]
62. Tredicucci A et al. *Appl. Phys. Lett.* **76** 2164 (2000)
63. Avrutsky I *Phys. Rev. B* **70** 155416 (2004)
64. Ramakrishna S A, Pendry J B *Phys. Rev. B* **67** 201101 (2003)
65. Lawandy N M et al. *Nature* **368** 436 (1994)
66. Lawandy N M *Appl. Phys. Lett.* **85** 5040 (2004)
67. Lawandy N M *Proc. SPIE* **5924** 59240G (2005)
68. Protsenko I E et al. *Phys. Rev. A* **71** 063812 (2005)
69. Sarychev A K, Shvets G, Shalaev V M *Phys. Rev. E* **73** 036609 (2006)
70. Sarychev A K, Tartakovsky G *Proc. SPIE* **6320** 63200A (2006)
71. Sarychev A K, Tartakovsky G *Phys. Rev. B* **75** 085436 (2007)
72. Sarychev A K, Pukhov A A, Tartakovsky G, in *Progress in Electromagnetics Research Symp.* (*PIERS*), *August 27–30, 2007, Prague, Czech Republic* (2007) p. 95; *PIERS Online* **3** 1264 (2007)


PACS numbers: **02.70.–c**, 42.25.Fx, 42.70.Qs
DOI: 10.3367/UFNe.0179.200909l.1027

# Application of the scattering matrix method for calculating the optical properties of metamaterials

N A Gippius, S G Tikhodeev

We consider the application of the scattering matrix formalism for calculating the eigenfrequencies, radiation widths, and field distributions of quasiwaveguide modes in photonic crystal layers (PCLs) of finite thickness.

At present, investigations are being performed of one-dimensional (1D) or two-dimensional (2D) periodic layers of photonic crystals whose vertical geometry can be arbitrarily complex [1–3]. Such PCLs have proved to be very interesting and promising structures; they can be prepared by the modern methods of layer-by-layer lithography; their optical properties are of practical interest in connection with their potential compatibility with microelectronic devices.

We note that PCLs are in fact diffraction gratings. Diffraction gratings play an extremely important role in optics and its applications. Therefore, their history, of course, is considerably older than the term 'photonic crystal.' The first diffraction grating was created and investigated by the American astronomer D Rittenhause in 1786 [4]. (The curious history of the creation of the first diffraction grating is described in [5].) But this discovery remained unnoticed, and in the majority of optics courses and encyclopedias, the creation of the diffraction grating (in 1821) is credited to Fraunhofer [6]. In 1902, Wood [7] experimentally detected narrow-frequency features in the reflection spectra of metallic diffraction gratings, which have been called Wood's anomalies since then. Two types of Wood's anomalies are distinguished. Diffraction anomalies, or Rayleigh anomalies [8], appear upon opening (with increasing frequency of incident light) new diffraction channels; the threshold frequency of opening a channel is characterized by the fact that the arising diffracted beam is parallel to the surface of the lattice (see also [9]). Resonance anomalies are connected with the excitation of resonance modes in the lattice, namely, surface plasmons or quasiwaveguide (Fabry–Perot) modes, depending on the type of structure. The qualitative laws governing the behavior of such resonances were first analyzed, as far as we know, by Fano [10]. Twenty years later, Fano in his famous work [11] analyzed the general laws governing the behavior of a discrete level in the background of the continuum; the arising asymmetric resonances are now called Fano resonances. Wood's resonance anomalies refer to precisely this type of resonance.

In view of the importance of the effect of the resonance optical response of diffraction gratings for many applications, including, for example, lasers with a distributed feedback, optical filters, and polarizers, this issue has been considered in an enormous number of studies. The majority of methods are based on the expansion of the scattered field of the diffraction grating in terms of three-dimensional Fourier harmonics (plane waves), as was first suggested by Rayleigh [8]. With the advent of computers, very powerful methods of calculation of optical spectra of arbitrarily complex diffraction gratings were developed. In this connection, we note the important work by Hessel and Oliner [12] and the development of the scattering matrix formalism in [13, 14]. Very powerful computational methods were developed [15] and [16], but, unfortunately, they are practically unknown to modern researchers working in this field.

A convenient method of constructing a scattering matrix for 1D or 2D PCLs with an arbitrarily complex structure in the direction perpendicular to the layer was developed in [17, 18]. The authors of these works extended the method of constructing the scattering matrix in [19] to electrodynamics for calculating electron tunneling in complex heterostructures. The scattering matrix method allows efficiently removing the numerical instabilities that appear in the method of transfer matrices because of the presence of exponentially decreasing and exponentially increasing linearly independent solutions. This method allows constructing a scattering matrix on the complex frequency plane [20] and developing efficient approximate descriptions of photonic resonances in such structures.

We note that the application of the scattering matrix method for metamaterials involves certain difficulties because of the poor convergence of Fourier series for the metal–dielectric structures. Recently, we succeeded in considerably improving the convergence of the method [21], using Li factorization rules [22] and the Granet method of adaptive spatial resolution [23], by supplementing the latter with a special curvilinear transformation of coordinates matched to the shape of the metal–dielectric interface.

The modes in a planar waveguide, as is known, have real eigenenergies $\Omega$, and the corresponding field distributions are localized near the waveguide layer and exponentially attenuate outside the waveguide. But in the case of a periodic modulation of the waveguide, a coupling of modes occurs with the continuum in the vacuum and in the substrate, and the quasiwaveguide modes acquire a finite radiation width. Only the waveguide modes with energies less than all diffraction thresholds remain undamped [24]. The spatial distributions of the electromagnetic fields of quasiwaveguide modes calculated at the natural *complex* frequency exponentially diverge as $z \to \pm\infty$. Although such solutions make no physical sense at first glance, a detailed analysis shows that this is not the case [15, 25]. These solutions increasing as $z \to \pm\infty$ have the physical meaning of eigenoscillations of the field in the waveguide that become damped in time; moreover, the solutions propagating into the vacuum and the substrate are finite because their exponential spatial growth is compensated by the decay of the eigenmode $\exp(-|\operatorname{Im}\Omega|\,t)$ damped in time. The space–time dependence of the solution, which is proportional to $\exp[|\operatorname{Im}\Omega|(z-ct)/c]$, describes the propagation of the front of the solution decaying in time.

In the theory of diffraction gratings, a traditional procedure is to construct the scattering matrix as a function of the complex propagation constant [13, 14] rather than the complex frequency [15]. The supporters of this approach believe that because the scattering matrix leads to 'nonphysical' solutions in the complex frequency plane, exponentially increasing in space, this method is mathematically inconsistent. Such increasing solutions have been known since the work of Thomson [26], who calculated the emission of an ideally conducting sphere. (For some reason, it has not been noticed that in constructing a scattering matrix as a function of the complex propagation constant, such exponentially increasing solutions also inevitably appear.) This apparent mathematical inconsistency, is removed by passing to nonstationary scattering, for example, to a decay; the exponential increase with moving away from the system is cut off by the exponentially decreasing time-dependent coefficient; as a result, the decay front moves with a limited amplitude. We also note that an essential advantage of constructing the scattering matrix in the complex frequency plane is the possibility of using causality relations.

The linear system eigenmodes are the nontrivial solutions of the equation

$$\mathbf{B}_{\text{out}} = S(\omega, \mathbf{k})\,\mathbf{B}_{\text{in}}\,, \tag{1}$$

which correspond to the zero vector of the amplitudes of the incoming waves $\mathbf{B}_{\text{in}}$. To find the eigenfrequencies of the system, it is necessary to find the scattering matrix on the complex plane. The causality principle ensures the absence of singularities in the scattering matrix on the upper half-plane of complex frequencies $\omega$; but the $S$ matrix can have poles at $\omega = \Omega - \mathrm{i}\gamma$, $\gamma \geqslant 0$, including those on the real axis. Such poles correspond to the decay of the mode in time at a rate proportional to $\propto \exp(-\mathrm{i}\Omega t - \gamma t)$ as $t \to \infty$, and $\gamma$ determines their inverse lifetime. For $0 < \gamma \ll \Omega$, these modes are associated with sharp changes in the transmission spectra of

the photonic crystal structure and with a strong resonance increase in the field near it.

For each fixed value of the wave vector in the **k** plane, $S$ matrix (1) as a function of $\omega$ on the complex plane can be obtained by an analytic continuation from the real $\omega$ axis on which it is defined uniquely [20]. We note that the analytic continuation of the $S$ matrix from the real $\omega$ axis to the lower half-plane depends on the choice of the axis interval limited by the points of opening of diffraction channels from which this continuation is performed. We consider this problem in more detail.

A two-dimensional diffraction grating couples the incident electromagnetic wave with a frequency $\omega$ and a wave vector $\mathbf{k} = (k_x, k_y, k_z)$,

$$k_x = \frac{\omega}{c}\sin\vartheta\cos\varphi,\ k_y = \frac{\omega}{c}\sin\vartheta\sin\varphi,\ k_z = \frac{\omega}{c}\cos\vartheta\,, \quad (2)$$

to all Bragg harmonics with the same frequency $\omega$ and the wave vectors

$$\mathbf{k}^{\pm}_{\mathbf{G},a} = (k_{x,\mathbf{G}}, k_{y,\mathbf{G}} \pm k_{z,\mathbf{G},a})\,, \quad (3)$$

where

$$k_{x,\mathbf{G}} = k_x + G_x\,,\ k_{y,\mathbf{G}} = k_y + G_y\,, \quad (4)$$

$$k_{z,\mathbf{G},a} = \sqrt{\frac{\omega^2\varepsilon_a}{c^2} - (k_x + G_x)^2 - (k_y + G_y)^2}\,, \quad (5)$$

($a = \mathrm{v}$ for the vacuum ($\varepsilon_\mathrm{v} = 1$) and $a = \mathrm{s}$ for a substrate), and

$$\mathbf{G} = \frac{2\pi}{d}\,(g_x, g_y, 0), \quad g_{x,y} = 0, \pm1, \pm2, \ldots \quad (6)$$

are the vectors of the reciprocal 2D lattice. In what follows, the following rule for choosing the square root sign is used: $\mathrm{Re}\sqrt{A} \geqslant 0$ for all complex $A$, and $\mathrm{Im}\sqrt{B} > 0$ for $\mathrm{Im}\,B = 0$ and $\mathrm{Re}\,B < 0$.

For a transparent nonabsorbing substrate, $\mathrm{Im}\,\varepsilon_\mathrm{s} = 0$. Under this condition, Bragg harmonics (3), depending on the frequency of the incident light $\omega$ (real number), are either propagating ($\mathrm{Im}\,(k_{z,\mathbf{G}}) = 0$) or exponential ($\mathrm{Re}\,(k_{z,\mathbf{G}}) = 0$). Below, the harmonics that exponentially increase (exponentially decay) when moving away from the PCL are called exponential (increasing or decaying). They should not be confused with the damped solutions for a two-dimensional photonic crystal inside the forbidden band. If $k^2_{z,\mathbf{G},a} > 0$, $a = \mathrm{v}, \mathrm{s}$, then the corresponding harmonics are the non-damped propagating solutions both in the vacuum and in the substrate. If $k^2_{z,\mathbf{G},\mathrm{v}} < 0$ and $k^2_{z,\mathbf{G},\mathrm{s}} > 0$, the harmonics are exponential in the vacuum and propagating in the substrate. Finally, if $k^2_{z,\mathbf{G},a} < 0$, then the corresponding harmonics are exponential on both sides of the PCL.

Thus, the $k^+_{\mathbf{G},\mathrm{v}}$ and $k^-_{\mathbf{G},\mathrm{s}}$ harmonics on the real $\omega$ axis, depending on whether the diffraction channel that corresponds to the reciprocal lattice vector **G** is open or is not open, are the solutions that either propagate toward the PCL or exponentially increase when moving away from it. They form a set of 'incoming' waves.

On the complex $\omega$ plane, the standard definition of the complex root in (5) for the 'propagating' harmonics, i.e., for $\mathrm{Re}\,k^2_{z,\mathbf{G},a} > 0$, has a cut below the negative real semiaxis (i.e., at $\mathrm{Re}\,k^2_{z,\mathbf{G},a} < 0$) and implies an analytic continuation of $k_{z,\mathbf{G},a}$ into the lower half-plane when $k^2_{z,\mathbf{G},a}$ intersects the *positive* real semiaxis, i.e., for open diffraction channels.

However, this cut prevents the analytic continuation of $k_{z,\mathbf{G},a}$ into the lower half-plane for closed diffraction channels. For these, it is therefore necessary to choose a cut in the definition of the square root differently, for example, to draw the cut under the *positive* real axis, as this is always done in the resonance theory.

Because the question of whether $k^2_{z,\mathbf{G},a}$ intersects the positive or negative real semiaxis as $\omega$ is shifted into the lower complex half-plane is equivalent to the question of whether the **G** diffraction channel is open or not at a given energy, the choice of the position of the square root cut is limited to the segment of the real axis of energies located between the adjacent diffraction thresholds.

The distribution of the amplitudes of the outgoing waves can be found by solving the homogeneous linear set of equations

$$RX = 0\,, \quad (7)$$

where $R \equiv S^{-1}$. As is well known, a homogeneous set of equations has a nontrivial solution only if its determinant is equal to zero. Therefore, dispersion curves are typically found by solving scalar equations equivalent to the vanishing condition for the determinant of the inverse scattering matrix as a function of $\omega$ and **k**. But in numerical calculations, it is much more convenient to use the method of linearization of the inverse scattering matrix (a variant of the multidimensional Newton algorithm), which is as follows.

Instead of solving a dispersion equation nonlinear in frequency,

$$\det R(\omega, \mathbf{k}) = 0\,, \quad (8)$$

which gives the spectra of eigenmodes $\omega(k)$ for linear system (7), it is necessary to calculate the inverse scattering matrix and its derivative with respect to energy at a certain point $\omega_0$ (for example, at the point where a certain state is obtained in the approximation of the empty lattice)

$$R_0 = R(\omega_0),\ R'_0 = \left.\frac{\partial R}{\partial\omega}\right|_{\omega=\omega_0}. \quad (9)$$

We then obtain

$$R(\omega) \approx R_0 + (\omega - \omega_0)\,R'_0\,. \quad (10)$$

Instead of solving system (7), we can, as the first iteration, find nontrivial solutions for the linear approximation of the inverse $S$ matrix in (10):

$$\left(R_0 + (\omega - \omega_0)\,R'_0\right)X = 0\,. \quad (11)$$

It can be seen that the last equation is equivalent to the *linear* problem for eigenvalues

$$-(R'_0)^{-1}R_0X = (\omega - \omega_0)\,X\,. \quad (12)$$

The computational effort for solving this linear problem is typically less than that required for calculating the inverse scattering matrix $R$. As a result, the $4N_\mathrm{g}$ eigenvalues $\delta_j$ are found, which give approximate values for the solutions of Eqn (7): $\Omega_j = \omega_0 + \delta_j$. The closer to the point of linear expansion $\omega_0$, i.e., the less the value of $\delta_j$, the more precise these approximation become.

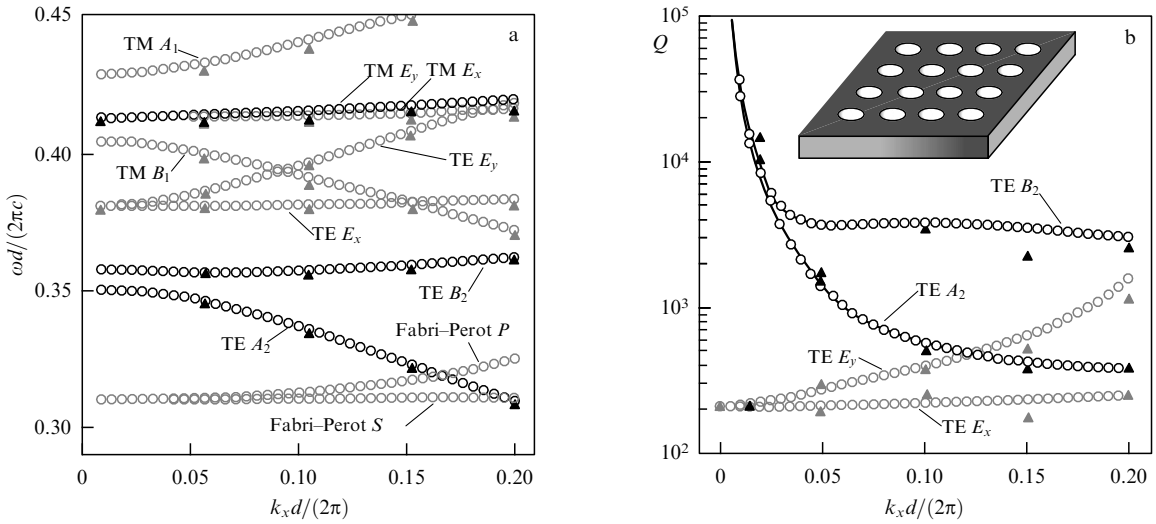


**Figure.** (a) Energies and (b) quality factors of quasiwaveguide modes of a photonic crystal layer schematically shown in the inset in Fig. 1b. The circles show the results of calculations by the scattering matrix method described in this paper; triangles correspond to the results of calculations by the finite-difference time-domain (FDTD) method [28].

The choice of the linear expansion point for the next iteration depends on which mode is sought and, correspondingly, which of the approximate solutions we should shift to. Typically, three iterations are found to be already sufficient for finding the nearest eigenvalue with a relative accuracy better than $10^{-5}$.

The advantages of this method are obvious; instead of the repeated cumbersome calculation of the $S$ matrix and the search for zeroes of the nonlinear scalar function of energy $\det R(\omega, \mathbf{k})$, which contains no information about the structure of the mode, we can implement the search by taking the structure of approximate modes into account, which allows a virtually complete automatization of data processing.

Furthermore, the 'remote' eigenvalues $\Omega_j$ and the corresponding vectors $X_j$ allow judging on the qualitative structure of the spectrum and symmetry of resonance states, because the procedure described preserves all the symmetry properties of the $S$ matrix.

If $X$ is an eigenvector and and $\Delta$ is the eigenvalue of the matrix $-(R_0')^{-1}R_0$, then by definition we have

$$-(R_0')^{-1}R_0X = X\Delta\,. \tag{13}$$

It follows from (13) that

$$R_0 = -R_0'X\Delta X^{-1}\,. \tag{14}$$

Substituting this expression in (10), we obtain approximations for $R(\omega)$ as

$$R(\omega) \approx R_0'X(\omega - \omega_0 - \Delta)\,X^{-1}\,, \tag{15}$$

and for the matrix $S(\omega) = R^{-1}(\omega)$ as

$$S(\omega) \approx X(\omega - \omega_0 - \Delta)^{-1}(R_0'X)^{-1}\,. \tag{16}$$

If we now choose $\omega_0$ to be the resonance energy of the multiplicity $n$ found above, then the first $n$ values $\Delta_{i,i}$ become zero and relations (16) allows explicitly isolating the resonance singularity in the scattering matrix.

We note in conclusion that in the case where the analytic continuation of the $S$ matrix into the lower half-plane from the chosen interval of the real $\omega$ axis has poles whose distance to the diffraction thresholds is more than the distance to the real axis, then in order to analyze the optical properties of the system in this energy range, it suffices to examine only the analytic continuation of the $S$ matrix from the selected interval. For example, this approach was used in [27] for an analysis of the manifestation of cell symmetry in the resonance features in the reflection spectra of PCLs. As an illustration of the capacity of this computational method, Fig. 1 shows the energies and the quality factors of the quasiwaveguide modes of a PCL schematically depicted in the inset in Fig. 1b (see also [29]). On the other hand, near the cutoff frequency of the quasiwaveguide mode, the poles of the scattering matrix closely approach the diffraction thresholds and begin to affect the spectral dependence of the $S$ matrix elements on the adjacent intervals of the real $\omega$ axis. Such behavior was first analyzed in [30].

Thus, we have demonstrated a very efficient method of calculating eigenfrequencies, radiation widths, and the distribution of fields of quasiwaveguide modes in photonic-crystal layers of a finite thickness, which is based on the scattering matrix formalism.

**Acknowledgments.** This work was supported in part by the Russian Foundation for Basic Research, the Presidium of the Russian Academy of Sciences, and the Division of Physical Sciences, Russian Academy of Sciences.

## References

1. Zengerle R *J. Mod. Opt.* **34** 1589 (1987)
2. Labilloy D et al. *Phys. Rev. Lett.* **79** 4147 (1997)
3. Astratov V N et al. *Phys. Rev. B* **60** R16255 (1999)
4. Rittenhouse D *Trans. Am. Philos. Soc.* **2** 202 (1786)
5. Bagbaya I D *Usp. Fiz. Nauk* **108** 335 (1972) [*Sov. Phys. Usp.* **15** 660 (1973)]
6. Fraunhofer J *Denkschr. König Akad. Wiss. München* **8** 1 (1821–1822)
7. Wood R W *Philos. Mag.* **4** 396 (1902)

8. Lord Rayleigh *Philos. Mag.* **14** 60 (1907)
9. Bolotovskii B M, Lebedev A N *Zh. Eksp. Teor. Fiz.* **53** 1349 (1967) [*Sov. Phys. JETP* **26** 784 (1968)]
10. Fano U *J. Opt. Soc. Am.* **31** 213 (1941)
11. Fano U *Phys. Rev.* **124** 1866 (1961)
12. Hessel A, Oliner A A *Appl. Opt.* **4** 1275 (1965)
13. Nevière M, in *Electromagnetic Theory of Gratings* (Ed. R Petit) (Berlin: Springer-Verlag, 1980) Ch. 5, p. 123
14. Nevière M et al. *Electromagnetic Resonances in Nonlinear Optics* (Amsterdam: Gordon and Breach Sci. Publ., 2000)
15. Shestopalov V P et al. *Rezonansnoe rasseyanie voln* T. 1: *Difraktsionnye Reshetki* (Resonance Wave Scattering. Vol. 1. Diffraction Gratings) (Kiev: Naukova Dumka, 1986)
16. Nikol'skii V V, Nikol'skaya T I *Dekompozitsionnyi Podkhod k Zadacham Elektrodinamiki* (Decompositional Approach to the Problems of Electrodynamics) (Moscow: Nauka, 1983)
17. Ager C D, Hughes H P *Phys. Rev. B* **44** 13452 (1991)
18. Whittaker D M, Culshaw I S *Phys. Rev. B* **60** 2610 (1999)
19. Ko D Y K, Inkson J C *Phys. Rev. B* **38** 9945 (1988)
20. Tikhodeev S G et al. *Phys. Rev. B* **66** 045102 (2002)
21. Weiss T et al. *Opt. Express* **17** 8051 (2009)
22. Li L *J. Opt. Soc. Am. A* **13** 1870 (1996)
23. Granet G *J. Opt. Soc. Am. A* **16** 2510 (1999)
24. Johnson S G et al. *Phys. Rev. B* **60** 5751 (1999)
25. Baz' A I, Zel'dovich Ya B, Perelomov A M *Rasseyanie, Reaktsii i Raspady v Nerelyativistskoi Kvantovoi Mekhanike* (Scattering, Reactions and Decay in Nonrelativistic Quantum Mechanics) (Moscow: Nauka, 1966) [Translated into English (Jerusalem: Israel Program for Scientific Translations, 1969)]
26. Thomson J J *London Math. Soc. Proc.* **15** 197 (1884)
27. Gippius N A, Tikhodeev S G, Ishihara T *Phys. Rev. B* **72** 045138 (2005)
28. Fan S, Joannopoulos J D *Phys. Rev. B* **65** 235112 (2002)
29. Tikhodeev S G et al. *Phys. Status Solidi C* **2** 795 (2005)
30. Lampariello P, Frezza F, Oliner A A *IEEE Trans. Microwave Theory Tech.* **38** 1831 (1990)